

THERMOMECHANICAL PROCESSING AND PRECIPITATION BEHAVIOUR IN 17-4PH STAINLESS STEEL

A Thesis Submitted
in Partial Fulfilment of the Requirements
for the Degree of
MASTER OF TECHNOLOGY

by

KALLOL BHATTACHARYYA

to the

DEPARTMENT OF MATERIALS AND METALLURGICAL
ENGINEERING
INDIAN INSTITUTE OF TECHNOLOGY
KANPUR

APRIL 1996

26 JUN 1996

CENTRAL LIBRARY

I. I. T., KANPUR

~~Acc. No. A. 121692~~

MME-1996-M-BHA-THE

A121692

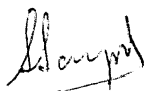
Dedicated

to

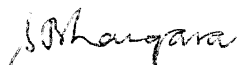
my parents

CERTIFICATE

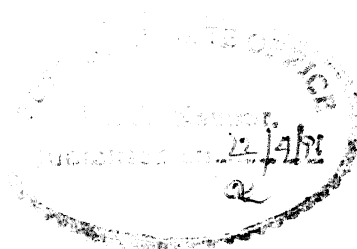
This is to certify that the present work, entitled “**Thermomechanical Processing And Precipitation Behaviour In 17-4PH Stainless Steel**” by Mr.Kallol Bhattacharyya has been carried out under my supervision and to the best of my knowledge it has not been submitted elsewhere for a degree.



Dr. S.Sangal
Assistant Professor
Dept. of Mat. & Met. Engg.
Indian Institute of Technology
Kanpur, UP 208 016.
INDIA.
Date-19.4.96



Dr. S.Bhargava.
Professor
Dept. of Mat. & Met. Engg.
Indian Institute of Technology
Kanpur, UP 208016.
INDIA.
Date-19.4.96



ACKNOWLEDGEMENT

I would like to express my sincere gratitude and appreciation to Prof.S. Bhargava and Prof.S. Sangal for their brilliant guidance and co-operation throughout the course of this work.

Among the others I am grateful to Mr. K. P. Mukherjee, Mr. P. K. Pal, Mr. U. S. Singh, Mr. V. K. Jain and Mr. H. C. Srivastava for assisting me at various stages of this work.

I cannot express my sincere gratitude towards Satyam Bhaiya and Sujatadi. Their help, constant encouragement and cooperation help me throughout this thesis work.

I am also thankful to my friends Rakshit, Manas, Anirban, Santanu and specially to Basuda.

I also acknowledge all those persons with whom I have had many days of pleasant association in the IIT campus.

Lastly, thanks are also extended to the head, all professors and staffs of the Dept. of Materials and Metallurgical Engg., IIT, Kanpur, for their active co-operation.

Kallol Bhattacharyya.

ABSTRACT

The different types of precipitates which are occurred in Z-174 precipitation hardening stainless steel are detected in this present study. It is found that precipitates may be of chromium and carbon or copper and nickel. Precipitation conditions of different types of precipitates depending on thermomechanical treatments have been studied also. Thermomechanical treatments given to different samples consist of giving different percentages of rolling at different temperatures or first ageing and then giving percentages deformation to the aged samples. The effect of natural ageing after giving high percentages deformations has been studied. It has been found that rolling and ageing at high temperature gives one intermetallic phase $\text{Cu}_{3.8}\text{Ni}$, volume percentage of which increases as the percentage deformation increases. The other types of precipitates are Cr_2C , Cr_3C_2 , Cr_7C_3 and Cr_{23}C_6 . Ageing at low temperature gives rise to one complex precipitate of the type $(\text{Cr}, \text{Fe})_7\text{C}_3$. Natural ageing is found to be very slow in this type of steel. Effect of different precipitate particles on the microhardness of the sample depending on their thermomechanical treatment has been studied also.

not needed
as you have already
said that diff. ppt
are obtained on diff. %
diff treatment

Contents

| | | |
|----------|--|-----------|
| 1 | INTRODUCTION | 1 |
| 2 | LITERATURE REVIEW | 3 |
| 2.1 | Evolution of Precipitation Hardened Stainless Steels . | 3 |
| 2.1.1 | Martensitic steels | 4 |
| 2.1.2 | Ferritic steels | 4 |
| 2.1.3 | Austenitic steel | 4 |
| 2.1.4 | Controlled transformation steels | 4 |
| 2.2 | Development of Controlled Transformation Stainless Steels | 5 |
| 2.2.1 | Basis of Metallurgical Design | 5 |
| 2.3 | Theoretical Basis of Precipitation-Hardening | 6 |
| 2.3.1 | Shape of Precipitates | 6 |
| 2.3.2 | Modulated Structures | 7 |
| 2.3.3 | Continuous And Discontinuous Precipitation . | 8 |
| 2.3.4 | Influence of Precipitation on Mechanical Properties | 12 |
| 2.4 | Precipitation -Hardening Stainless Steels | 22 |
| 2.4.1 | The Tempering of 17-4 PH Steel | 25 |
| 2.4.2 | The Formation of Alloy Carbides During Secondary Hardening | 25 |
| 2.5 | Application of 17-4PH Stainless Steels | 25 |
| 2.6 | Fe-Cr-Ni Phase Diagram | 26 |
| 3 | EXPERIMENTAL PROCEDURE | 28 |
| 3.1 | Materials and their preparation | 28 |
| 3.2 | Processing Details and Parameters | 28 |
| 3.2.1 | Austenitizing | 28 |

| | | |
|-------|--|--|
| 3.2.2 | Thermomechanical Processing | |
| 3.3 | Characterisation Techniques | |
| 3.3.1 | Electron Probe Microanalysis | |
| 3.3.2 | Scanning Electron Microscopy | |
| 3.3.3 | X-Ray Diffraction | |
| 3.3.4 | Hardness Measurement | |

4 RESULTS AND DISCUSSIONS

| | | |
|-------|--|--|
| 4.1 | Chemical Composition of the as Received Material . | |
| 4.2 | X-Ray Diffraction | |
| 4.2.1 | Analysis From X-Ray Data of the Sample A1 . | |
| 4.2.2 | Analysis from X-Ray Data of the sample A3 . | |
| 4.2.3 | Analysis from X-Ray Data of the sample C1 . . | |
| 4.2.4 | Analysis from X-Ray Data of the sample C3 . . | |
| 4.2.5 | Analysis from X-Ray Data of the sample P1 . . | |
| 4.2.6 | Analysis from X-Ray Data of the sample D1 . | |
| 4.3 | Analysis of the SEM Microstructures | |
| 4.4 | Results Obtained from Hardness Measurement | |

5 CONCLUSIONS

List of Tables

| | | |
|-----|---|----|
| 2.1 | Compositions of various types of precipitation hardened stainless steels | 23 |
| 2.2 | Mechanical properties of various types of precipitation hardened stainless steels depending upon thermomechanical treatment | 24 |
| 3.1 | Composition of the steel as specified by MIDHANI . . | 28 |
| 3.2 | Details of thermomechanical treatments given and sample designation | 30 |
| 4.1 | Standard X-ray data for possible precipitates | 35 |
| 4.2 | X-Ray Analysis Table For Sample A1 | 37 |
| 4.3 | X-Ray Analysis Table For Sample A3 | 40 |
| 4.4 | X-Ray Analysis Table For Sample C1 | 40 |
| 4.5 | X-Ray Analysis Table For Sample C3 | 42 |
| 4.6 | Comparison Of Various X-Ray Analysis Results | 45 |
| 4.7 | Hardness Values For First Rolled And Then Aged Samples | 56 |
| 4.8 | Hardness Values For First Aged And Then Rolled Samples | 56 |

List of Figures

| | | |
|------|---|----|
| 2.1 | Diagram of a cell formation through discontinuous precipitation at a migrating boundary | 11 |
| 2.2 | Dependence of CRSS on particle size | 14 |
| 2.3 | Passage of a dislocation pair through a crystal containing ordered precipitate | 16 |
| 2.4 | Effect of the presence of precipitates with lower stacking fault energy | 17 |
| 2.5 | Dependence of CRSS on precipitate size according to Hirsch and Kelly's theory | 19 |
| 2.6 | Schaeffler Diagram | 27 |
| 3.1 | Thermomechanical processing schedules | 31 |
| 4.1 | X-Ray chart for the sample A1 | 36 |
| 4.2 | X-Ray chart for the sample A3 | 38 |
| 4.3 | X-Ray chart for the sample C1 | 39 |
| 4.4 | X-Ray chart for the sample C3 | 41 |
| 4.5 | X-Ray chart for the sample P1 | 43 |
| 4.6 | X-Ray chart for the sample D1 | 44 |
| 4.7 | X-Ray chart for the sample D1 | 44 |
| 4.8 | X-Ray chart for the sample D1 | 44 |
| 4.9 | X-Ray chart for the sample D1 | 44 |
| 4.10 | X-Ray chart for the sample D1 | 44 |
| 4.11 | Microstructure of the as received sample | 46 |
| 4.12 | Microstructure of the sample which is 50% rolled at 1080°C and aged at 480°C | 46 |
| 4.13 | Microstructure of the sample which is 70% rolled at 1080°C and aged at 480°C | 47 |

have these figures?

| | | |
|------|---|----|
| 4.14 | Microstructure of the sample which is 70% rolled at 1080°C and aged at 580°C | 47 |
| 4.15 | Microstructure of the sample which is 30% rolled at 1080°C and aged at 580°C | 48 |
| 4.16 | Microstructure of the sample which is 50% rolled at 1080°C and aged at 580°C | 48 |
| 4.17 | Microstructure of the sample which is 50% rolled at 1080°C and aged at 580°C | 49 |
| 4.18 | Microstructure of the sample which is 70% rolled at 1080°C and aged at 580°C | 49 |
| 4.19 | Microstructure of the sample which is aged at 580°C . | 50 |
| 4.20 | Microstructure of the sample which is aged and rolled to 30% at 580°C | 50 |
| 4.21 | Microstructure of the sample which is aged and rolled to 50% at 580°C | 51 |
| 4.22 | Microstructure of the sample which is aged and rolled to 70% at 580°C | 51 |
| 4.23 | Microstructure of the sample which is aged and rolled to 30% at 480°C | 52 |
| 4.24 | Microstructure of the sample which is aged and rolled to 50% at 480°C | 52 |
| 4.25 | Microstructure of the sample which is aged and rolled to 70% at 480°C | 53 |
| 4.26 | Microstructure of the sample which is 40% rolled at 1080°C and naturally aged | 53 |
| 4.27 | Microstructure of the sample which is rolled to 50% and aged at 300°C | 54 |
| 4.28 | Microstructure of the sample which is rolled to 30% and aged at 300°C | 54 |
| 4.29 | Hardness Vs. Ageing Temperature Plot For The Samples Which Are First Rolled And Then Aged | 56 |
| 4.30 | Hradness Vs. Ageing Temperature Plot For The Samples Which Are First Aged And Then Rolled | 57 |

Chapter 2

INTRODUCTION

Precipitation hardened stainless steels are important corrosion resistant structural material. These steels are used in air craft skin and missile casings and various other similar applications. The high strength to weight ratio, high strength upto 600°C , high impact toughness, weldability and machinability makes them comparable with strength^{*} Al-Li alloys. Al-Li alloys suffer from variation in strength in different directions due to texture effect. But precipitation hardened stainless steels do not show such behaviour. So, these steels attract attention as an important material for research.

Precipitation hardened (PH) stainless steels are of three types-1. austenitic 2. semi - austenitic (austenite + martensite) 3. martensitic. 174PH which is used in this present study belongs to the group of martensitic grades. These steels are usually solution annealed at the mill and supplied in that condition. Solution treatment temperature for this type of steel ranges from $1050-1100^{\circ}\text{C}$. Solution treatment and air cooling produces martensite. Ageing is carried out by heating in the temperature range of $450-600^{\circ}\text{C}$. Ageing gets completed within 18 hours. Four different heat treatments are used for Z-174 steels. They can be classified as :- 1. H 900°F (482°C) 2. H 1025°F (552°C) 3. H 1075°F (580°C) 4. H 1150°F (620°C). Heat treatment conditions are specified by the temperature at which the steels are heated after solution treatment and air cooling. Ageing improves both toughness and resistance to stress corrosion cracking. Properties achieved depend on the heat treatment condition because distribution and types of precipitate depend on heat treatment condition. But what are the types of precipitates and how their occurrence depend on thermomechanical conditions and heat

treatment condition that is not studied in the previous works. |

During ageing various types of precipitates occur depending upon the condition of heat treatment. Rolling at high temperature and ageing gives rise to precipitation of $\text{Cu}_{3.8}\text{Ni}$ intermetallic phase. More and more $\text{Cu}_{3.8}\text{Ni}$ gets precipitated out with increasing percentage of deformation. Chromium carbides such as 1. Cr_2C 2. Cr_3C_2 3. Cr_7C_3 4. Cr_{23}C_6 get precipitated during ageing. Low temperature ageing gives complex precipitate of the type $(\text{Cr.Fe})_7\text{C}_3$. Due to strain field associated with
→ coherent precipitate of $\text{Cu}_{3.8}\text{Ni}$, maximum hardness is associated with the condition of high temperature rolling and ageing.

Knowledge of the types and condition of precipitates which are detected and determined in this present study will help in the further development associated with this steel.

Chapter 2

LITERATURE REVIEW

2.1 Evolution of Precipitation Hardened Stainless Steels

The most important property of high chromium stainless steels is their corrosion resistance. General level of mechanical properties and forming characteristics can be equalled or exceeding by many other types of steels at a much lower cost. But these type of stainless steels were only developed for their high corrosion and oxidation resistance. The stainless steels are mainly used for both corrosion resisting and high temperature creep resisting or heat resisting application. As chromium content in steel increases, temperature of application also increases. For creep resisting application these steels are suitably alloyed to produce required creep strength.

Design criteria for stainless steels can be noted as below:

1. corrosion and oxidation resistance in the operating environment
2. mechanical and physical properties
3. fabrication characteristics from the point of view of both hot and cold working
4. weldability and welding must not impair the corrosion resistance, creep resistance or general mechanical properties.

Stainless steels can be classified as below.

2.1.1 Martensitic steels

They contain 12 - 17% chromium, 0-4% nickel, 0.1 - 1.0% carbon, and sometimes addition of molybdenum, vanadium, niobium, aluminium and copper. These are alloyed to give required tempering resistance and strength. Their austenitizing temperature depends on alloy content (usually 900 - 1100°C), and high hardenability makes them martensitic air hardenable even in large section sizes. This gives difficulty in machining and fabrication as they are frequently alloyed to produce required degree of tempering resistance. So, these steels are frequently tempered to produce required degree of ductility, toughness and precipitation hardening.

2.1.2 Ferritic steels

They contain 15 - 30% chromium, low carbon, no nickel and sometimes addition of alloying elements like molybdenum, titanium or niobium. These are highly corrosion resistant, show little or no transformation and are formable.

2.1.3 Austenitic steel

They contain 18 - 25% chromium with 8 - 20% nickel and low carbon contents. These steels are often alloyed with molybdenum, niobium or titanium and are predominately austenitic at all temperatures. Some amount of delta-ferrite may be present depending upon composition. The austenite may have a varying degree of stability with respect to the formation of martensite, being transformed by cold work ~~work~~ at room temperature in some compositions. Other compositions are stable down to -196°C and are not transformed by the most severe deformation.

2.1.4 Controlled transformation steels

They contain 14-17% chromium, up to 7% nickel and sometimes additions of alloying elements such as molybdenum, aluminum, copper, titanium etc. These are austenite at the solution-treatment temperature but the

M_s temperature can be adjusted by various thermo-mechanical treatments so that they can be either metastable austenite or martensite at room temperature. Subsequent tempering produces room temperature. Subsequent tempering produces martensite. During tempering an age hardening reaction can be introduced.

Precipitation hardening stainless steels are in the group of controlled transformation stainless steels.

2.2 Development of Controlled Transformation Stainless Steels

2.2.1 Basis of Metallurgical Design

Controlled transformation stainless steels were developed for the requirement of aircraft industry for a high strength steel which could be used for the skin of high speed aircraft. These steels are ~~are~~ easily fabricable and weldable and maintain ^{their} ~~its~~ strength in the welded condition and at temperature as high as 400°C . In order to have a strength/weight ratio equivalent to highest strength of aluminium alloys, it should have a minimum strength of 1100 MN/m^2 . This strength can also be achieved by ¹² fabricate in heat treated condition. Cold worked ferritic or austenitic steels can produce the required strength, but they would suffer from varying strength when fabricated and loose strength after welding or during prolonged service at 400°C . ^{lose}

Therefore these steels should be soft and ductile when in sheet form and then it should be uniformly hardenable after fabrication. ~~This can be~~ This can be obtained by ~~an~~ age-hardening austenitic steels, but to get the required amount of strength the steel must be solution-treated at high temperature which is expensive. Attention was thus turned to an austenitic steel capable after fabrication of being transformed to martensite by a fairly low temperature heat treatment which would not cause any distortion. These steels must be capable of being strengthened by a low temperature precipitation-hardening treatment of martensite.

The basic requirements for designing these types of stainless steels are [1]:

1. a steel with a soft austenitic structure after solution treatment and air cooling from temperature not exceeding 1100°C , in order to facilitate cold working and fabrication
2. sufficient tempering resistance to have the strength upto the temperature of 400°C
3. ability to introduce precipitation-hardening at temperatures below 600°C
4. weldability
5. a low carbon content to prevent corrosion by weld-decay and to get maximum formability. Niobium or titanium is added to get maximum stabilization against weld-decay
6. sufficient chromium for corrosion resistance
7. a limited amount of delta ferrite to maintain high strength and prevent low ductilities in the heat affected zone.

2.3 Theoretical Basis of Precipitation-Hardening

2.3.1 Shape of Precipitates

The main shapes of precipitates from the solid solution in age hardening alloys are fine-lamellar (usually of disc-shaped), equiaxed (usually spherical or cubic) and acicular.

The shape of a precipitate is determined by two rivalling factors, i.e. surface energy and elastic energy due to strain, both tending to reach a minimum. Since the surface energy tends to its minimum, there is a tendency of formation of equiaxed precipitates and of appearance of faceted forms with the least surface tension at all the faces. The elastic strain energy is the lowest with the fine lamellar precipitates. Thus the shape of precipitates will tend to be either equiaxed or fine lamellar depending on which of these two factors prevail.

The elastic strain energy increases as the mismatch between the precipitate and matrix increases. When the difference of atomic diameters of the components in a solid solution does not exceed 3%, the

shape of precipitate is determined by minimum of surface energy and is close to spherical. While the difference $\geq 5\%$, the elastic strain energy predominates and fine lamellar or disc shaped particles occur.

Coherent precipitates may sometimes be of acicular shape, which corresponds to elastic strain energy which is higher than that of disc shaped particles ~~but lower than that of disc shaped particles~~ but lower than that of the equiaxed precipitates.

In F.C.C solid solutions, coherent lamellar precipitates are often located along $(1\ 0\ 0)$ plane of the matrix. This may be explained by an anisotropic modulus of elasticity of such a matrix; the normal modulus of elasticity is at its minimum along $\langle 1\ 0\ 0 \rangle$ directions, i.e., the deformation along these directions is at its maximum, which ensures the lowest strain energy.

When an incoherent precipitate forms, tangential stresses are absent, but normal stresses appear always, since different specific volume of the matrix and the precipitate inevitably cause hydrostatic compression or tension[2].

2.3.2 Modulated Structures

As the elastic strain energy due to distortion tends to minimum, it can influence the mutual disposition of the precipitates, as well as their shape. Upon the precipitation from solid solution, this tendency of elastic strain energy is conducive in some alloys to the formation of so called modulated or periodic structures, which can be characterised by a regular spatial disposition of coherent precipitates spaced at definite distance from each other, this distance being called the modulation period of a structure, λ . Modulation period is generally not more than a few hundreds of interatomic spacing.

In some alloys modulated structures can appear at the earliest stages of precipitation, for instance, during spinodal precipitation, while in others they may appear a certain time after the precipitation has started. As the ageing time is increased, a modulated structure may first become even more pronounced and then gradually transform into a combination of chaotically located precipitates, which usually occurs owing to coagulation of particles and the loss of coherency.

The morphology of modulated structures in various alloys can be different depending on the conditions of heat treatment. In some cases there may be thin lamellar precipitates spaced at equal distances and parallel to a crystal plane; in others there may be periodically disposed rod like precipitates forming a three dimensional network of overlapping rods which are parallel to a definite direction in the matrix. For example, the elastically soft $[1\ 0\ 0]$ direction in cubic crystals. Such a network of precipitates is usually seen as a "basket-interlacking" pattern. Most typical variety of modulated structure is the one formed by rows of cubic precipitates parallel to the $[1\ 0\ 0]$ direction of the cubic lattice matrix [2].

2.3.3 Continuous And Discontinuous Precipitation

Continuous Precipitation

With continuous precipitation, individual precipitates of an excess phase form and grow in the ~~in the~~ initial supersaturated solution. Since these precipitates are enriched in one of the the components, the matrix ~~phase~~ is relatively depleted of that component and ~~a~~ a concentration gradient is present in it.

Crystals of the excess phase grow owing to common downhill diffusion: the flow of atoms is directed towards decreasing concentration and the diffusion coefficient D is positive.

During continuous precipitation the alloying element gradually comes out from the matrix phase and precipitates grow in size. The matrix is depleted of that alloying element throughout the whole volume down to equilibrium concentration C_a .

As the ageing time t with continuous precipitation increases, the size r of precipitate increases approximately as:

$$r = Dt^{1/2} \quad (2.1)$$

According to microstructural features, continuous precipitation of a solution during ageing may be classed into general and localized.

With general precipitation, the precipitates are uniformly distributed over the volume of grains. Nucleation may be either homogeneous or

heterogeneous (if the preferable sites of the nucleation are distributed uniformly throughout the bulk of the grains).

When localized precipitation occurs, the distribution of precipitates throughout the bulk of grains is non-uniform. Precipitation is always heterogeneous and occurs at grain boundaries, slip bands and other preferential sites [3].

Discontinuous Precipitation

With discontinuous precipitation, or nodules of a two phase mixture $\alpha_1 + \beta$ nucleate and grow inside grains of the initial supersaturated solid solution α_s . The α_1 phase inside the cells has the same lattice as the initial α_s -phase, but its composition is an equilibrium one at a given temperature of preparation or is intermediate between initial and equilibrium composition. *spelling*

$$\alpha_s \rightarrow \alpha_1 + \beta \quad (2.2)$$

The average composition of the two phase mixture $\alpha_1 + \beta$ in a cell is the same as that of the initial solution α_s .

During the transformation, the concentration of the initial solution \rightarrow remains all the time unchanged until the solution disappears fully. In a narrow zone between a cell and initial solution there occurs an abrupt jump of the concentration: from the initial concentration to inside the cell.

Discontinuous precipitation is always localized and starts most often at grain boundaries. The crystal orientation of α_1 - phase in a cell differs from the initial orientation of α_s - phase in the grains inside which the cell is growing. On the other hand, the orientation of phase in the cell is the same as in neighbouring grains at the other sides of the boundary, where discontinuous precipitation has started. Thus, the motion of the front of a cell in discontinuous precipitation towards a grain is accompanied with a reorientation of the crystal lattice of the matrix phase can be regarded as the motion of an of an intergranular boundary towards the grain that is being consumed. The thermodynamic stimulus for this motion is the difference between the volume

free energy of the initial supersaturated solution and that of the two phase mixture inside the cell.

The mechanism of formation of a cell in discontinuous precipitation is still not clear enough. According to a theory which is based on the structure of the structure of the transformation it may be reduced to following. As a grain boundary migrates, a dissolved element precipitates near it in form of particles which locally pin the boundary. When migrating further, the boundary bends between precipitates and the later are stretched during their growth and follow the moving boundary. This process forms alternate layers of α_1 and β phase. (Fig. 2.1)

The mechanism of growth of the precipitate can be described as below. The concentration of an alloying element B at the end faces of plates or rods of α_1 and β phase is respectively increased or reduced. Discontinuous precipitation causes the components to redistribute diffusively along the interface between the matrix and the cell. Discontinuous precipitation can proceed rapidly at low temperature because of small interplate distance in the cells which decreases with lowering temperature of ageing.

Magnesium alloys based on the Mg-Al-Zn system (such as GRADE MJ 15) and austenitic ferrous alloys (such as GRADE 36 HXTIO) show discontinuous precipitation.

In ageing, discontinuous precipitation is usually avoided where possible, since the two phase structure with incoherent precipitates that forms on it is coarser and respectively less strong than that obtained through common precipitation hardening which forms coherent or semicoherent disperse precipitates. Besides, incoherent lamellar precipitates of an excess phase at grain boundaries may have an embrittling effect on alloys.

Discontinuous precipitation can sometimes produce a useful effect if it forms a phase coherent with the matrix, such as γ -phase (of the Ni_3Al type) in alloy GRADE 36 HXTIO, ageing results in the formation of a disperse structure and improved mechanical properties of the metal [3].

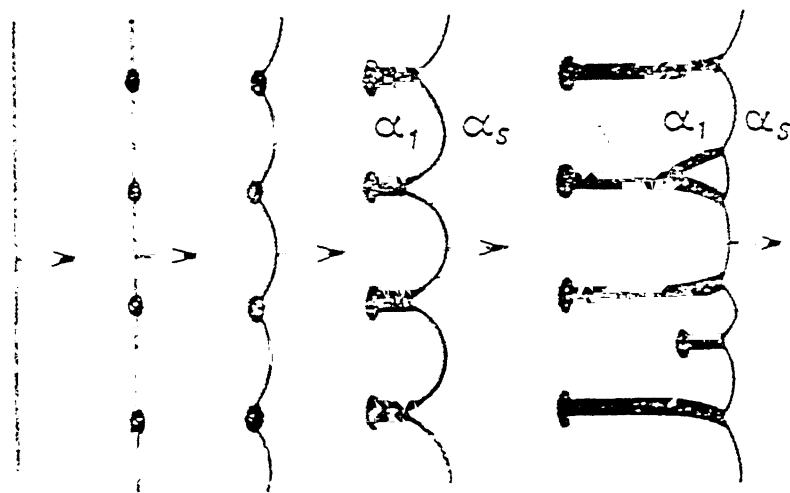


Figure 2.1: Diagram of a cell formation through discontinuous precipitation at a migrating boundary

2.3.4 Influence of Precipitation on Mechanical Properties

Precipitation changes both the physical and mechanical properties of the alloys. Theories of precipitation hardening as appeared in various papers can be summarized as below.

Strengthening Due To Misfit Stresses

The lattice is sometimes strained to give close matching across the interface between the matrix and the precipitate. This gives rise to internal strain field which hinder the field of the gliding dislocations. ~~field of the gliding dislocations.~~ Hardening from misfit is important in case of non-ideal G.P. zones where the solute atoms differ considerably in size from the solvent. The dislocation theory of strengthening from misfitting precipitates is suggested by Mott and Nabarro [4]. They suggested that for the dislocation to pass through regions of internal stress, the average stress must be at least equal to the average internal stress field. Assuming the precipitates to be spherical the CRSS for such a crystal can be calculated as:

$$\tau = 2G[1 - r_b/r_a] \quad (2.3)$$

where G = the shear modulus, f = the volume fraction of the precipitate and r_a and r_b are the atomic radii of the matrix and precipitate respectively. If the precipitate is not spherical the result will be the same but with a different numerical constant. ~~Their theory can also explain,~~ By considering the extent to which dislocation can bow between particles under the action of a given stress, the existence a critical size of dispersion for maximum hardening, *can also be explained.*

Sterengthening Due to Cutting of Particles by Dislocations

Glide dislocations are often seen [5-9] to cut through small precipitates. When a dislocation shears the precipitates, hardening may result due to one or more of several factors. Fleischer [10,11], pointed out that variation of elastic moduli between the precipitate and matrix may be a source of strengthening. If the shear modulus of the particle is larger than that of the matrix, an extra stress will be required

to force the dislocation through the particle. However a detailed theory considering this effect has not been developed. The slip planes in the particle may not be continuous with those in the matrix. Slip can continue in the particle by creating jogs[12] or nucleating separate interface dislocations[13]. So in both the cases increased stress is required to cause plastic flow to occur. When the dislocation cuts the precipitate ~~there is precipitate~~ there is an increase in precipitate-matrix interface area. So additional work in the form of applied stress whose magnitude is determined by surface area per unit area of the interface, must be done to force the dislocation through ~~done to force the dislocation~~ through the precipitate. Coherent precipitate with low surface energy can easily be sheared. Non-coherent precipitates have high surface energy and cannot be easily sheared.

Strengthening With Ordered Precipitate

The moving dislocation can either cut or by pass precipitate particles. The changes in CRSS due to coherent particles shows dependence on particle size for a constant volume fraction of precipitate according to Fig. 2.2. Dislocation intersection mechanism changes from cutting to by-pass at a critical size. If the coherent ordered precipitate have no elastic strain field around them, only the cutting mechanism is known to be operative irrespective of the particle size. Gerold and Haberkorn[14] calculated the strengthening due to coherency strain and obtained the expression:

$$\tau = 3G\epsilon^{3/2}(Rf/b)^{1/2} \quad (2.4)$$

where ϵ = constrained lattice strain, R = the mean particle radius and b = the Burgers vector.

Another source of strengthening lies in the fact that dislocation move in pairs, thus creating antiphase boundaries (APB), if the particles possess long range order. Under stress the first dislocation sees more of APB as result of bowing between particles (Fig. 2.3). The second dislocation is generally straight. Strengthening occurs due to difference in the amount of APB seen by the first and second dislocations. The second dislocation will be pulled forward the APB energy, E , of the par-

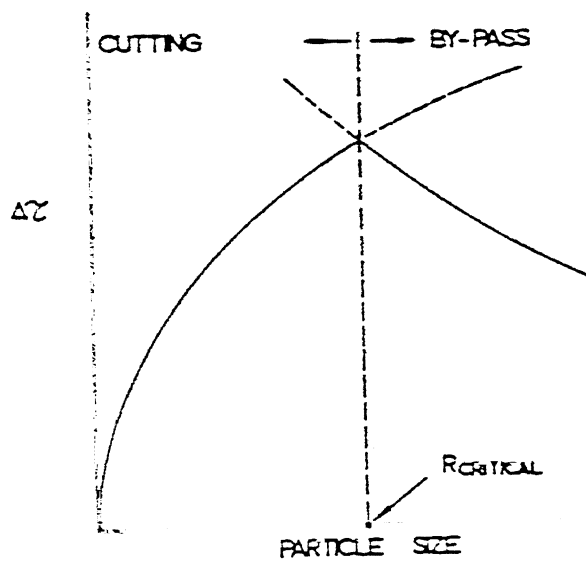


Figure 2.2: Dependence of CRSS on particle size

ticle it cuts by a force equal to Ef . The force on the first dislocation is thus $2\gamma_b + Ef$. From this CRSS can be calculated and is given by [15]:

$$\tau = \frac{A/E^{3/2} f^{1/2} r^{1/2}}{bU^{1/2}} - \frac{fE}{2b} \quad (2.5)$$

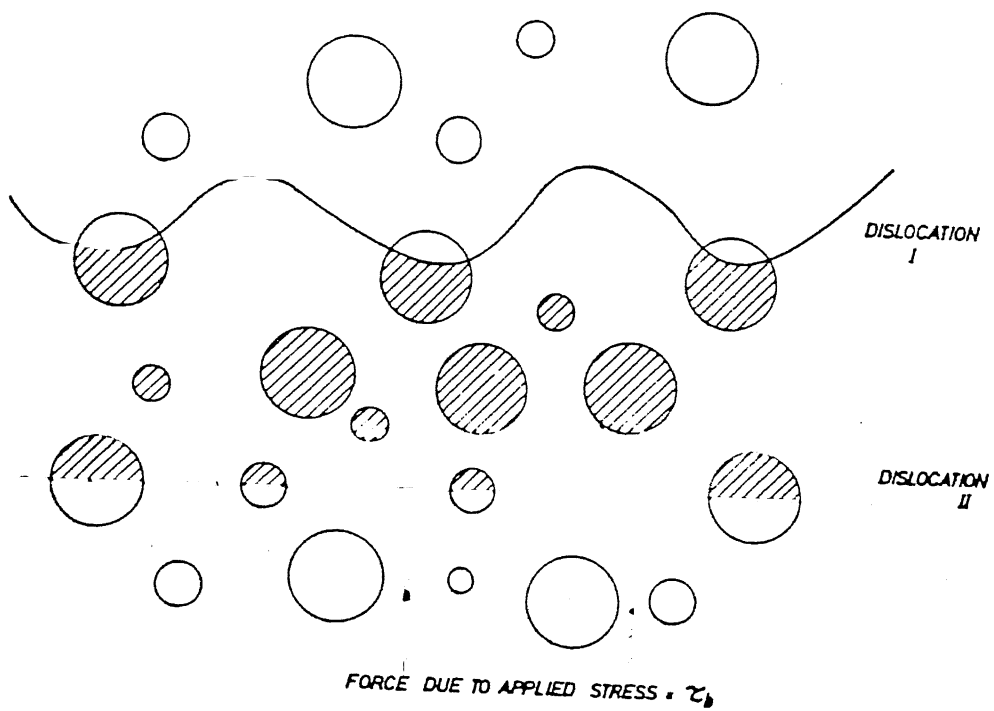
where U = line tension of the dislocation and A is a constant which depends on the geometrical distribution of the particles. The above equation assumes that APB energy is the equation assumes that APB energy is the only resistance to dislocation motion. It is reasonable to believe in any case that strengthening in alloys with ordered particles is mainly due to either of the APB energy and strain fields or both. Large ordered precipitate particles are again by passed and when this happens a transition occurs from pair to single dislocation flow.

Stacking Fault Strengthening (SFE)

Hirsch and Kelly [16] have proposed another mechanism of strengthening in a precipitation system based on a difference in the SFEs between the matrix and the precipitate. The addition of solute atoms in metals alter the SFEs. If the distribution of the solute is not uniform, the dislocation will be attracted towards those regions where the SFE and hence the dislocation energy is lower. If an alloy has segregated into zones and if the SFE in the zone is lower than that in the matrix, then a dislocation will tend to take the form shown in Fig. 2.4 so as to pass through as many particles as possible. Work must then be done to pull away the dislocation from the particles and this will increase the yield stress. If the SFE is higher in the precipitate then the dislocation is repelled by them and avoids passing through them as far as possible.

The stress needed to move a dislocation in such an alloy can be calculated from: (1) the work done by the elastic force per unit length of the dislocation when the separation of partial dislocation changes from w_1 to w_2 and (2) the force required to move a dislocation from the precipitate. The yield stress is found to depend on the relative sizes of the width of the extended dislocation and the particles in the slip plane. The following cases will be considered:

1. when the average diameter, $2r$, of the section of the particle in



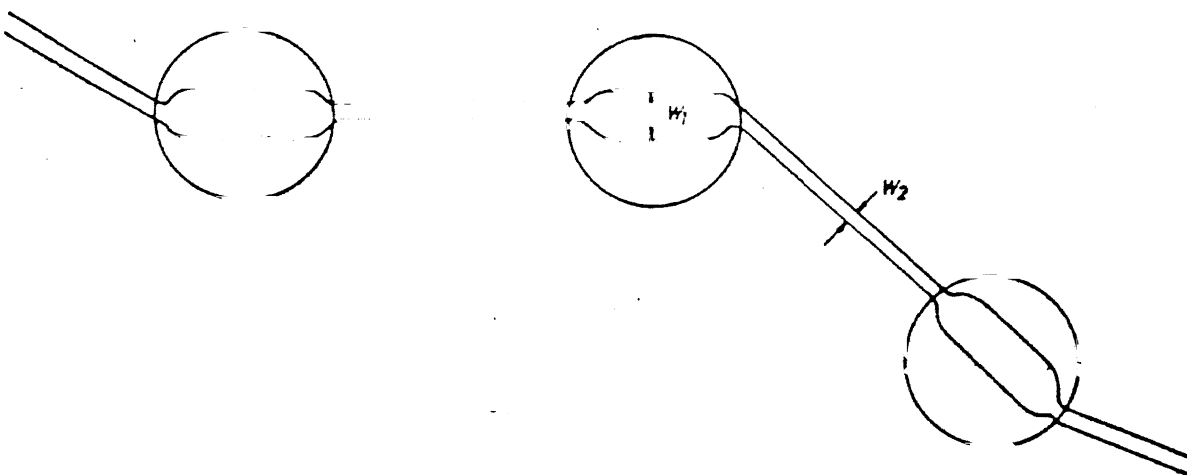


Figure 2.4: Effect of the presence of precipitates with lower stacking fault energy

the slip plane is greater than the two stacking fault widths, the CRSS is given by

$$\tau \propto R^{-1/2} f^{2/3} \quad (2.6)$$

where R is the radius of the particle,

2. where $2r$ is less than the width w_2 ,

$$\tau \propto R^{1/3} f^{2/3} \quad (2.7)$$

3. in the intermediate case i.e., for $w_2 < 2r < 2W$ where W is the average stacking fault width, the model predicts that τ is almost independent of R but proportional to $f^{2/3}$. However with increasing R in this range the interaction energy between the particle and dislocation increases and consequently τ exhibits a slight increase with increasing R . The variation of τ with r for a given f is shown in Fig.2.5. At very small values of $2R$, τ abruptly decreases to zero.

The yield stress of a precipitation hardened alloy, the strength of which is solely due to stacking fault effect, should vary with R for a constant fraction of precipitates and at a constant temperature as follows: at small particle sizes, $2R < (6f/\pi)^{1/2} w_2$, no strengthening will be observed. Above this value of R the yield stress increases with increasing value of R (yield stress is proportional to $R^{1/3}$) until $2R = (3\pi/8)w_2$. Beyond this limit, yield stress will increase rather slowly to a maximum which will occur somewhere between $2R = (3\pi/8)w_2$ and $2R = w_1$. For values of $2R > w_1$, the yield stress decreases as $R^{-1/2}$. The maximum value of yield stress depends on the difference in the SFEs in the matrix and the precipitate. This effect is therefore important in the matrices of high SFE such as Al and Ni containing precipitate particles.

Another important aspect of the influence of stacking faults is borne out by studies [17-22] on austenitic steels alloyed with some

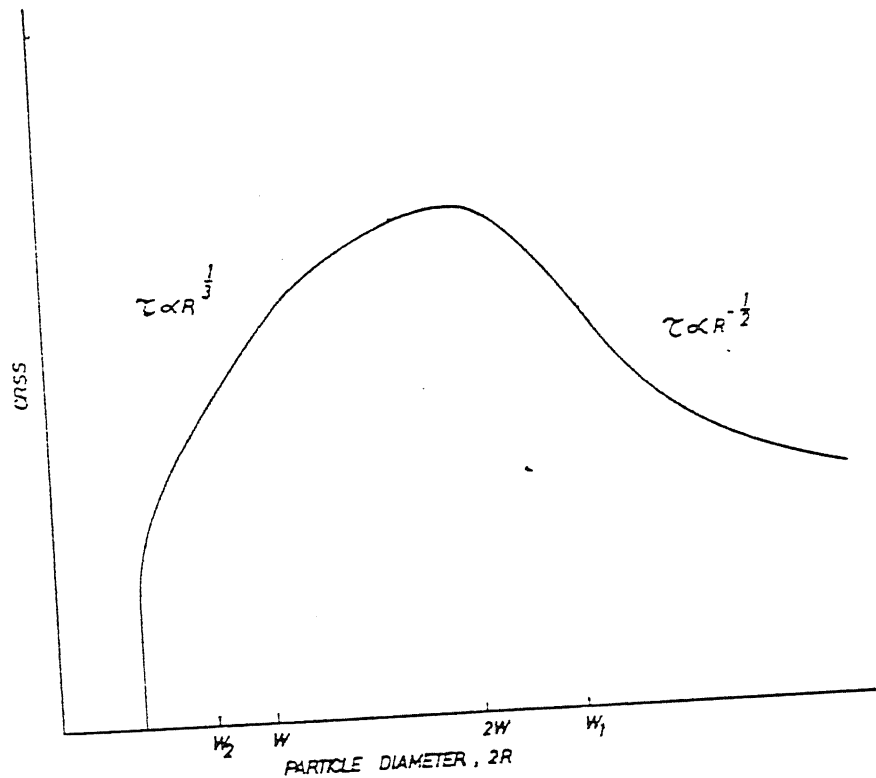


Figure 2.5: Dependence of CRSS on precipitate size according to Hirsch and Kelly's theory

amount of Nb,V,Ti,Ta etc. Precipitation of carbides is found to be accompanied by the nucleation and growth of stacking faults. Silcock and Tustall[20] found, when investigating precipitation of NbC in a 17/12 steel that the extrinsic type of stacking fault bounded by a Frank and a Schockley partial dislocation are nucleated. The presence of such extended stacking faults and the extrinsic faults contribute in some measure to the overall strengthening.

Yield Stress of an Alloy Containing Nondeforming Particles

Large incoherent precipitates cannot be sheared by the dislocation because of extensive increase in the surface energy. The glide dislocation may avoid the particle by leaving the slip plane in the vicinity of each particle[23]. It may also avoid the particle by Orowan mechanism[24]. In this mechanism, it is assumed that the precipitate do not deform the matrix. They serve as the pinning points and the dislocation has to bend between the particles leaving a dislocation ring about each particle. In both the above cases energy must be supplied to increase the total length of dislocation line and hence yield stress of a crystal containing nondeforming particle is hence higher. The Orowan mechanism gives the stress necessary to expand a loop of dislocation between particles as:

$$\tau = \tau_s + 2U/b\lambda \quad (2.8)$$

where τ is the yield stress of the matrix and λ is the spacing between the precipitates in the slip plane. In the overaged state λ increases at constant volume fraction of the precipitate and hence the yield stress decreases. The model thus explaining the decrease in yield stress after long ageing times.

Ansell and Lenel[25] on the other hand suggest that glide dislocations pile up against the particle until the stress concentration at the head of pile-up is sufficient to yield or fracture the particle. The resulting increase in flow stress is proportional to $\lambda^{-1/2}$. This model does not enjoy much experimental support and considerable strengthening may be achieved without the particles yielding or fracturing.

A theory for hardening of metals based on the free energy considerations of a specimen in which the matrix flows uniformly while the

precipitate deforms elastically is developed[26]. The amount of plastic deformation inside and outside the particle is different and consequently there arises an internal stress, this is referred to as "internal stress effect"[27,28]. In addition, the precipitate has different elastic moduli from those of the matrix which will give rise to additional stress fields. The stress state of matrix is thus different from that of uniformly deforming materials without the particles. This is thought to be the cause of hardening by non deforming particles. The hardening rate is predicted to be proportional to the volume fraction but independent of particle size.

Work Hardening with Precipitation Hardened Alloys

The strain hardening rate in alloys with precipitates is dictated by the interaction dislocation with particles of given ^{7 1 1 1 1}and distribution. The controlling factors seems to be whether the particles are sheared or are avoided. The hardening rate when the dislocations cut ^{8 1 1}through the precipitates, as in the case with small closely spaced coherent particles, is ^{9 1 1}comparable with that of pure metal[7,9,29,30]. This is due to the fact ^{10 1 1}there is no increase in the length of the moving dislocation subsequent to cutting. However, the alloy crystals may have a slight ^{11 1 1}higher work-hardening rate than metals with no precipitate because of two main factors: (1) the SFE of the precipitate is usually lower than in the matrix[16] thereby making cross slip difficult and (2) when a dislocation passes through the precipitate an interface dislocation may be left behind; the stress field of this dislocation opposes the motion of the glide dislocation on the same and neighbouring slip plane resulting in an increase in work hardening rate. Hence soft precipitate particles through which dislocation can pass result in a work hardening behaviour similar to pure metal with only slightly higher work hardening rates.

The work hardening rate in alloys containing nondeformable particles is much more rapid[7,29,30]. The moving dislocation bypasses such hard particles leaving a dislocation loop around the particle. There is then an increase in the total dislocation length per unit volume of the crystal. Fisher, Hart and Pry[31] proposed that accumulation of dislocation loops around particles gives rise to a back stress, which requires

the application of higher stress to force the glide dislocations between particles.

Thermally Activated Plastic Flow in Alloys with Precipitates

The flow stress of metals with small precipitate particles is a function of temperature, as in case with pure metals and single-phase materials, so that the shear strain rate, $\dot{\gamma}$, may be expressed as:

$$\dot{\gamma} = P \exp[-H(\tau)/kT] \quad (2.9)$$

The stress dependence of H can be deduced as [32]:

$$\tau = \frac{H_o}{V} \left[1 - \left(\frac{kT}{H_o} \ln \frac{P}{\dot{\gamma}} \right)^{2/3} \right] \quad (2.10)$$

where H_o is a stress-dependent activation energy, $P = N A b \nu$, N = the number of points per unit volume at which dislocations are held up at successful fluctuation, ν = the frequency of vibrations of the dislocation, k = Boltzmann's constant, T = temperature in absolute scale.

2.4 Precipitation -Hardening Stainless Steels

As a result of research on controlled transformation stainless steels, a new group of stainless steels with precipitation hardening characteristics were developed. In 1948 the first of these group 17-7PH was made available. These steels are usually solution annealed in the mill and supplied in that condition. After forming they are aged to attain the increase in hardness and strength. Low nickel content in these stainless steels reduces the stability of austenite. Copper and aluminium tend to form coherent alloy precipitates. Typical combinations of various types of stainless steels are given in Table 2.1.

The 17-4PH alloy is solution treated at 1100°C followed by air cooling with the resultant transformation of austenite to martensite. Ageing is carried out by reheating in the temperature range of 450 - 600°C to cause precipitation hardening. The 17-4PH steel is not used in application in solution treated condition because of its low ductility and poor resistance to stress corrosion cracking.

| Alloys | C | Mn | Si | Cr | Ni | Mo | Cu | Al |
|--------|------|-----|-----|------|-----|-----|----|-----|
| 17-4PH | | | | | | | | |
| (a) | 0.04 | 0.5 | 0.2 | 16.5 | 3.5 | 3.5 | — | — |
| (b) | 0.10 | 0.5 | 0.2 | 17.0 | 4.0 | 2.0 | — | — |
| 17-7PH | 0.07 | 0.5 | 0.2 | 17.0 | 7.0 | — | — | 1.1 |
| 15-7PH | 0.07 | 0.5 | 0.2 | 15.0 | 7.0 | 2.5 | — | 1.2 |

Table 2.1: Compositions of various types of precipitation hardened stainless steels

The 17-7PH and PH 15-7 Mo alloys are solutioned- annealed at 1100°C followed by air cooling. ~~This~~ This treatment produces a structure of austenite with about 5 to 20 percent delta ferrite.

Research papers show that four different heat-treatments were employed on 17-4PH stainless steel. They can be classified as[33]-

1. H 900°F
2. H 1025°F
3. H 1075°F
4. H 1150°F

1. H 900°F: { Heat treatment schedule is as given below } solution treated at 1100°C → air cooling → reheating to 900°F (482°C)
2. H 1025°F: solution treated at 1100°C -- → air cooling → reheating to 1025°F (552°C)
3. H 1075°F: solution treated at 1100°C - → air cooling → reheating to 1075°F (580°C)
4. H 1150°F: solution treated at 1100°C → air cooling → reheating to 1150°F (621°C)

Mechanical properties of this steel due to heat treatment is given in Table 2.2.

Several hardening sequences are prescribed for 17-7 PH and PH 15-7 Mo. In TH sequence, the austenite is conditioned ~~to~~ by reheating to 760°C which ~~which~~ produces precipitation of chromium

| GRADE | CONDITION | TENSILE STRENGTH PSI | 0.2% YIELD STRENGTH PSI | REDUCTION OF AREA % |
|----------|-----------|----------------------------|-------------------------------|---------------------------|
| 17-4PH | annealed | 150,000 | 110,000 | 45 |
| | H900°F | 200,000 | 178,000 | 48 |
| | H1025°F | 170,000 | 165,000 | 56 |
| | H1150°F | 145,000 | 125,000 | 60 |
| | H1075°F | 165,000 | 150,000 | 58 |
| 17-7PH | annealed | 130,000 | 40,000 | — |
| | TH1050°F | 200,000 | 185,000 | — |
| | RH950°F | 235,000 | 220,000 | — |
| | CH950°F | 265,000 | 260,000 | — |
| PH15-7Mo | annealed | 130,000 | 55,000 | — |
| | TH1050°F | 210,000 | 200,000 | — |
| | RH950°F | 240,000 | 225,000 | — |

Table 2.2: Mechanical properties of various types of precipitation hardened stainless steels depending upon thermomechanical treatment (Source)?

carbides. Precipitation reduces chromium and carbon contents of the austenite and allows transformation on cooling. Cooling is continued to below 16°C but above 0°C in order to obtain the amount of martensite necessary for the strength level desired. Ageing is usually carried out at 566°C for the best combination of strength and ductility. The TH sequence gives better ductility but lower strength than other sequences. In RH sequence the austenite is conditioned at 954°C. This higher temperature results in more carbon in solution in the austenite therefore a lower M_s temperature. The transformation to martensite is obtained by a subzero treatment at - 74°C with subsequent ageing at 510°C. The 17-7 PH steel may be supplied in the cold rolled condition which helps in transformation and heat treatment reduces to a single ageing at 510°C. Although strength is greatly increased, but ductility and formability is reduced[33].

2.4.1 The Tempering of 17-4 PH Steel

In principle, the changes in structure during tempering are similar to the 12% Cr steel. The retarded softening is associated with the formation of a fine precipitate M_2X which coarsens as the tempering progresses but does not appear to form plates or needles during overageing. The rapid softening at temperatures of 500 - 550°C is presumed to be the result of loss of coherency and the formation of $M_{23}C_6$ at grain boundaries.

Further softening takes place as the $M_{23}C_6$ grows with increased time or higher tempering temperatures until interrupted by re-austenitization.

The M_2X phase is hexagonal and in this steel has been identified. It is possible that it forms as a transitional phase to Cr_7C_3 with perhaps a deficiency of Cr, but owing to the rapid formation of $M_{23}C_6$ never changes to Cr_7C_3 [34].

2.4.2 The Formation of Alloy Carbides During Secondary Hardening

Very early in the secondary process alloy carbides are formed as cloud like mass of particles. These alloy carbides are of a very fine size. Such a precipitate causes hardening by coherency straining of the lattice. These coherent precipitates are closely analogous to G.P. zones observed in precipitation hardening aluminium-base alloys, which are of a similar size.

Overageing starts at grain boundaries and is followed by the formation of larger plates or needles from the fine dense precipitate which causes ~~in~~ a loss of coherency. Eventually these dissolve in the presence of a more thermodynamically highly alloyed carbides that form later in the tempering process. This loss of dispersion hardening results in a further decrease in hardness [34].

2.5 Application of 17-4PH Stainless Steels

17-4PH stainless steels are used in the design of aircraft and missiles. The unique feature of high strength/weight ratio is obtained by

honeycomb structure. Cores for these structures are made by bonding formed strips together to make square or hexagonal configuration. These shapes are brazed together.

The brazing mixtures should have the following qualities:

1. Good thermal conductivity.
2. Resistance to thermal shock in all sizes.
3. Ability to hold flatness or contours.

→ Brazing is done in helium or argon atmosphere. Brazing mixture consists of 85% Ag and 15% Mn [35].

2.6 Fe-Cr-Ni Phase Diagram

The Fe-Cr-Ni diagram is shown in Fig 2.6. This model does not give details of composition and temperature [36], and is not drawn exactly to scale. The range of stability of the δ -phase extends in the form of a tunnel closed at one end and with thick walls. The open end of this tunnel lies on the iron-chromium boundary of the ternary diagram, the other end being closed where the $\alpha + \gamma$ fields meet the pure δ area. The inner tunnel is at first a single phase zone, but becomes duplex ($\gamma + \delta$) where it enters $\alpha + \delta$ region. The walls of the tunnel have at first a duplex $\delta + \gamma$ structure. Later the walls consist of triangular areas of $\alpha + \gamma + \delta$, the thickness of these walls tending to diminish both the "open" and "closed" ends of the tunnels.

→ Stable phases at room temperature in steels containing Cr and Ni can also be determined from well known Schaeffler diagram modified by Schneider (Fig-2.7) [37]. The chromium and Nickel equivalents are ;

Cr
→ Chromium equivalent = $(\text{Cr}) + 2(\text{Si}) + 1.5(\text{Mo}) + 5(\text{V}) + 5.5(\text{Al}) + 1.75(\text{Nb}) + 1.5(\text{Ti}) + 0.75(\text{W})$, Nickel equivalent = $(\text{Ni}) + (\text{Co}) + 0.5(\text{Mn}) + 0.3(\text{Cu}) + 25(\text{N}) + 30(\text{C})$ where the brackets indicate the weight percent of the alloying element.

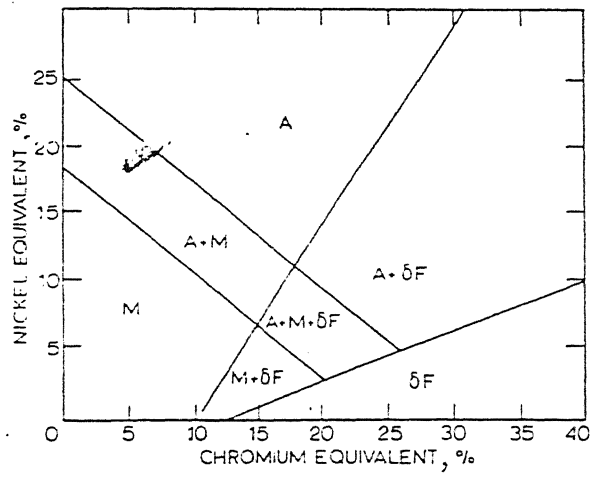
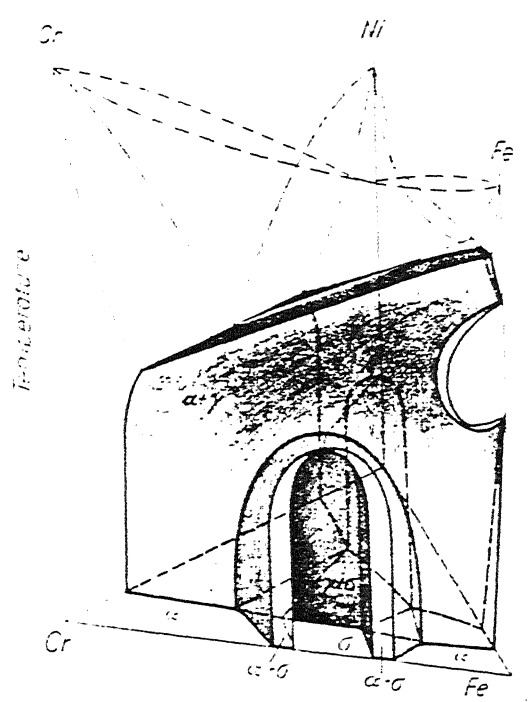


Figure 2.6: Schaeffler Diagram

Chapter 3

EXPERIMENTAL PROCEDURE

3.1 Materials and their preparation

A steel block of Z-174 precipitation hardened stainless steel supplied by MISHRA DHATU NIGAM LIMITED, Hyderabad was used as the starting material for the present research work. The composition of this steel as mentioned by MIDHANI are given in Table-3.1.

The block was of initial dimentions 26Cm X 10Cm X 2Cm. From it small pieces of dimentions 15mm X 15mm X 10mm were cut and used for this study.

3.2 Processing Details and Parameters

3.2.1 Austenitizing

It is reported in the literature that austenitizing temperature for this type of steel ranges from 1050-1100°C and the precipitation occurs at the temperature range of 450-600°C. The full ageing time is reported as 18 hour and this is used in the present study. All the samples were austenitized at 1080°C for 1 hour in this work.

| C | Mn | Si | Cr | Ni | Cb | Cu |
|------|-----|-----|------|------|------|------|
| 0.04 | 0.4 | 0.5 | 16.5 | 4.25 | 0.25 | 3.60 |

Table 3.1: Composition of the steel as specified by MIDHANI

3.2.2 Thermomechanical Processing

To study the effect of prior deformation on ageing two temperatures were selected (1080°C and 300°C) and after austenitizing and air cooling the samples were rolled at these temperatures and three percentage deformation 30%, 50% and 70% were given. High temperature rollings were done by giving 10% deformation in each pass to reduce the sample thickness to the desired thickness. Low temperature rollings were done by giving 5% deformation in each pass. Then the samples were aged at two different temperatures (580°C and 480°C).

To study the effect of deformation on the precipitated particles, the samples after austenitizing and air cooling were aged at 580°C and 480°C and then rolled 30%, 50% and 70% to those temperatures by giving 5% deformation in each pass. All the thermomechanical treatments are shown in Fig 3.1. Details are given in Table-3.13.

Effect of natural ageing in this steel has been studied after rolling 40% and 70% at high temperatures (1080°C and 900 °C), air colling and then allowing sufficient time for the samples to be naturally aged.

The austenitizing and preheating for hot rolling of specimens was done in a horizontal muffle furnace. The furnace was having a constant temperature zone of about 15-20 Cm in length and was heated by carbide rods. Muffle of the furnace consisted of an inconel tube, 750 mm long and of 100 mm internal diameter, and was closed from one end. The furnace was mounted on wheels and a had a protrusion which could be brought up to the nip of the rolls.

Hot rolling was done on a two high rolling mill which had 135 mm diameter rolls. Speed of rotation for hot rolling mill was kept as 55 rpm in all the experiments. For austenitizing, ageing or heating prior to rolling samples were placed on a tray and then pushed carefully into the constant temperature zone of the furnace and heated for the desired time.

| SAMPLE | THERMOMECHANICAL TREATMENT GIVEN |
|--------|---|
| A | Soaked for 1h at 1080°C,air cooled,aged for 18h at 580°C and then 30%(A1),50%(A2) and 70%(A3) rolled. |
| B | Soaked for 1h at 1080°C,30% (B1),50%(B2)and 70% rolled at that temperature.air cooled and aged for 18h at 480°C |
| C | Soaked for 1h at 1080°C,30% (C1),50%(C2)and 70% rolled at that temperature.air cooled and aged for 18h at 580°C |
| C4 | Soaked at 1080°C for 1h,air cooled and aged at 580°C for 18h |
| D | Soaked at 1080°C for 1h,air cooled,30%(D2)and 50% (D1)rolled at 300°C and then aged at 300°C |
| Q | Soaked at 1080°C for 1h,air cooled,aged at 480°C for 18h and 30%(Q1),50%(Q2) and 70% rolled at 480°C |
| P | Soaked at 1080°C for 1h, 40%(P1) and 70%(P3) rolled at that temperature and then naturally aged |

Table 3.2: Details of thermomechanical treatments given and sample designation

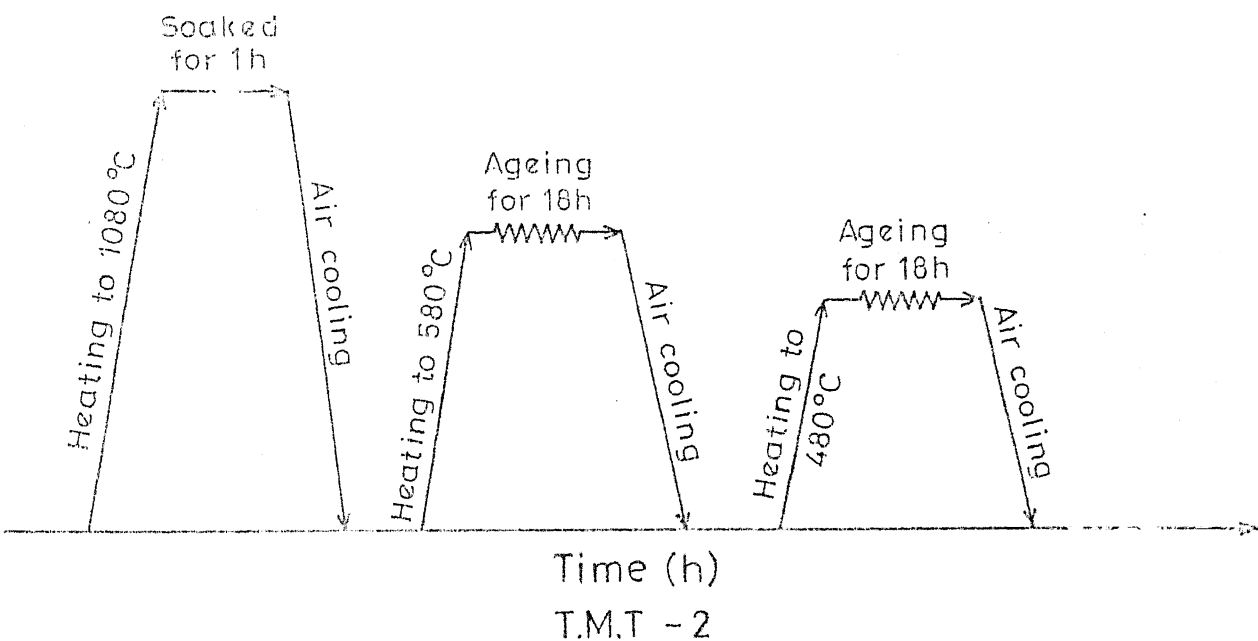
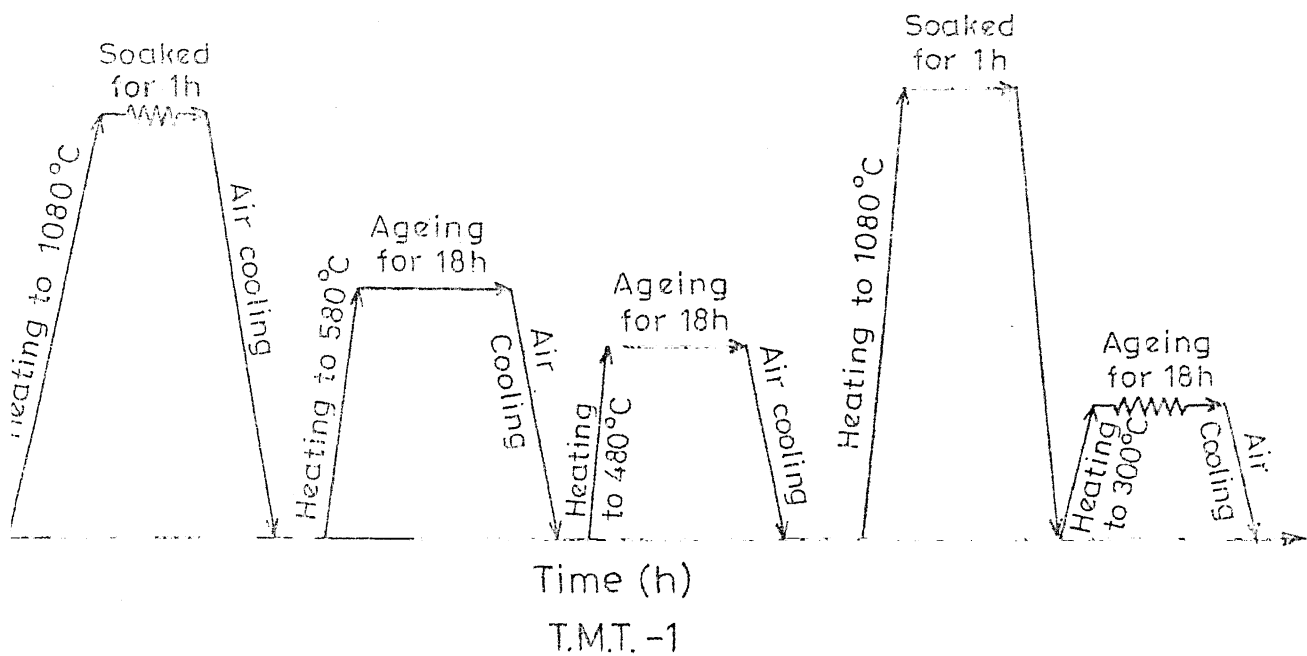


Figure 3.1: Thermomechanical processing schedules

3.3 Characterisation Techniques

3.3.1 Electron Probe Microanalysis

Since these types of steels are of non-standard grades and a range of composition for different elements were given in literature, so, EPMA was done to know the exact composition of the steel used. EPMA was done in a JXA-8600 electron probe microanalyser at four arbitrary points.

3.3.2 Scanning Electron Microscopy

Scanning electron microscopy (SEM) was carried out using a JEOL (JSM-840A) for all the samples. The samples were cut into small pieces and mounted separately within cold setting resin for scanning electron microscopy. After mounting, these samples were subjected to conventional metallographic grinding, polishing and then etching by Fry's reagent [$\text{CuCl}_2=5\text{g}$, $\text{HCl}=40\text{ml}$, $\text{H}_2\text{O}=30\text{ml}$, Methyl Alcohol= 25ml]. Photographs were taken at different magnifications from different regions of etched surface by using secondary mode or back scattering mode.

3.3.3 X-Ray Diffraction

X-Ray analysis was done by using "SEIFERT ISO DEBYFLEX 2002" X-Ray diffractometer. The samples were analysed using CuK_α radiation, source speed as $3^\circ/\text{min}$ or $0.3^\circ/\text{min}$, charge speed as $0.6\text{ cm}/\text{min}$ and cpm as 2K or 5K. Peaks for possible precipitates were identified for analysis.

3.3.4 Hardness Measurement

Micro-hardness for all the samples were measured by using a micro-hardness tester of the model Leitz Microhardness Tester (Miniload-2). The dimensions of the indentations were measured and the hardness were determined from the standard chart.

Chapter 4

RESULTS AND DISCUSSIONS

It has been shown in the literature review that the austenitizing temperature for this type of steel ranges from 1050-1100°C. It is also reported that the temperature at which precipitation occurs lies between 450-600°C. In the present study the austenitizing temperature was kept as 1080°C. The effect of prior deformation on precipitation and the effect of deformation on the precipitated particle has been studied. Effect of natural ageing on the prior deformed sample has also been studied. All the samples were aged for 18 hour of steel. 777

As mentioned earlier, the chemical composition of precipitates and condition of their formation in 17-4PH steel have not been properly investigated. It is reported in some literature that precipitate may be of chromium and carbon[34] or may be of copper and nickel[33]. From chromium carbon phase diagram it can be concluded that chromium carbides may be of the following types-1. Cr_2C 2. Cr_3C_2 3. Cr_7C_3 4. Cr_{23}C_6 and one complex precipitate of the type 5. $(\text{Cr},\text{Fe})_7\text{C}_3$. Similarly binary copper-nickel phase diagram shows complete solid solution over the whole range of compositions with no intermetallic compound formation in Cu-Ni system. Precipitate composition of copper and nickel is not mentioned in the literature. Due to presence of other alloying elements copper and nickel may give intermetallic phase.

4.1 Chemical Composition of the as Received Material

EPMA is carried out at four arbitrary points in the as received sample keeping carbon, manganese and niobium percentage fixed since their standards are not available.

From the EPMA result the average composition of the steel is obtained as-

Cr=15.460 - 15.949%, Ni=3.627 - 3.869%, Cu=2.64 - 3.14%, Si=0.499 - 0.538%, C=0.04%, Mn=0.4%, Nb=0.25%, Fe=Balance. All the above percentages are given in weight percentages.

4.2 X-Ray Diffraction

As mentioned previously, various chromium carbides belonging to Cr-C system namely Cr_2C , Cr_3C_2 , Cr_7C_3 , Cr_{23}C_6 and a complex carbide belonging to Fe-Cr-C system namely $(\text{Cr}, \text{Fe})_7\text{C}_3$ may form in the 17-4PH stainless steels. However, their precipitation is likely to be influenced by the conditions existing in the alloy which are favourable to their nucleation and growth. Those conditions in turn, are likely to be effected by the processing schedules which influences sub-structural details of the microstructures. The occurrence of precipitation of these carbides and/or intermetallic compound was studied by analysing differently processed alloy samples using X-ray diffraction method.

The standard X-ray diffraction data obtained from JCPD files has been summarized in table-4.1. The presence of a given precipitate in a sample was confirmed by analysing the data obtained from it and comparing with the standard data. These results are given below.

4.2.1 Analysis From X-Ray Data of the Sample A1

Thermomechanical treatment of the sample: Soaking for 1h at 1080°C cooling → Ageing for 18h at 580°C → 30% rolling at 580°C.

X-Ray chart for this sample is shown in the Fig.4.1.

From the X-Ray chart it is clear that precipitate phases are- 1. $\text{Cu}_{3.8}\text{Ni}$
2. Cr_2C 3. Cr_3C_2 4. Cr_7C_3 5. Cr_{23}C_6

| Phase | 2θ in $^{\circ}$ | Plane |
|-------------------------------------|----------------------------|-------|
| Cr_7C_3 | 44 | 1 5 1 |
| | 42 | 1 1 2 |
| | 39 | 1 5 0 |
| Cr_2C | 28 | 0 0 2 |
| | 52 | 1 1 2 |
| | 48 | 1 1 0 |
| Cr_3C_2 | 39 | 1 2 1 |
| | 40 | 2 3 0 |
| | 48 | 2 2 1 |
| Cr_{23}C_6 | 44 | 5 1 1 |
| | 41 | 4 2 2 |
| | 37 | 4 2 0 |
| $(\text{Fe},\text{Cr})_7\text{C}_3$ | 46 | 1 5 1 |
| | 43 | 1 1 2 |
| | 41 | 1 5 0 |
| $\text{Cu}_{3.8}\text{Ni}$ | 44 | 1 1 1 |
| | 51 | 2 0 0 |
| | 91 | 3 1 1 |

Table 4.1: Standard X-ray data for possible precipitates

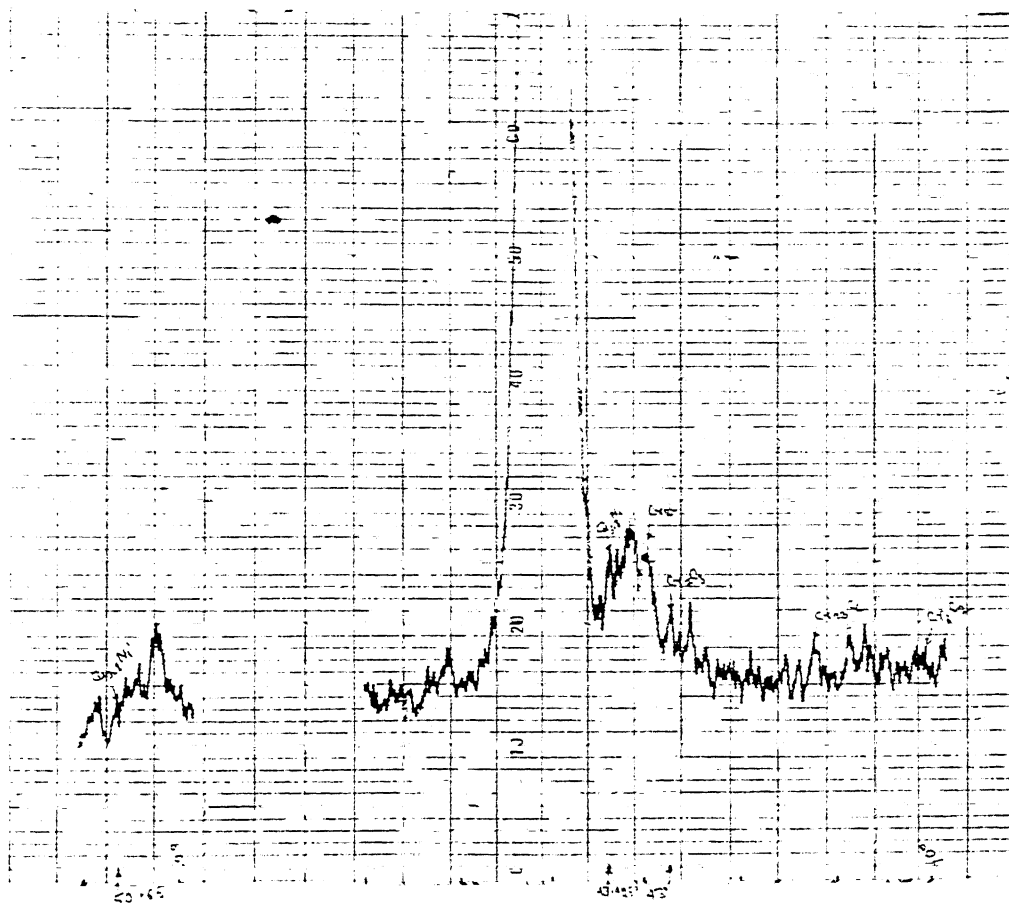


Figure 4.1: X-Ray chart for the sample A1

| Different phases present | Height of 100% intensity of different phases(cm) | I_{max}/I_{phase} |
|--------------------------|--|---------------------|
| $Cu_{3.8}Ni$ | 0.25 | 0.057 |
| Cr_2C | 4.17 | 1.0 |
| Cr_7C_3 | 3.65 | 0.875 |
| Cr_3C_2 | 3.73 | 0.895 |
| $Cr_{23}C_6$ | 2.26 | 0.543 |

2. This is the data for diff. components

Table 4.2: X-Ray Analysis Table For Sample A1

Ratios of height of the 100% intensity of different precipitate phases with respect to 100% intensity of the maximum precipitated phase are given in table-4.2.

4.2.2 Analysis from X-Ray Data of the sample A3

Thermomechanical treatment of the sample: Soaking for 1h at 1080°C

→ Air cooling → Ageing for 18h at 580°C → 70% rolling at 580°C

X-Ray chart for this sample is shown in the Fig.4.2.

From the X-Ray chart it is clear that precipitate phases are- 1. $Cu_{3.8}Ni$
2. Cr_2C 3. Cr_3C_2 4. Cr_7C_3 5. $Cr_{23}C_6$

Ratios of height of the 100% intensity of different precipitate phases with respect to 100% intensity of the maximum precipitated phase are given in table-4.3.

4.2.3 Analysis from X-Ray Data of the sample C1

Thermomechanical treatment of the sample: Soaking at 1080°C for 1h → 70% rolling at 1080°C → Air cooling → Ageing for 18h at 580°C

X-Ray chart for this sample is shown in Fig.4.3.

From X-Ray chart it is clear that precipitate phases are- 1. $Cu_{3.8}Ni$
2. Cr_2C 3. Cr_3C_2 4. Cr_7C_3 5. $Cr_{23}C_6$ Here $Cu_{3.8}Ni$ is the maximum precipitating phase.

what does this mean

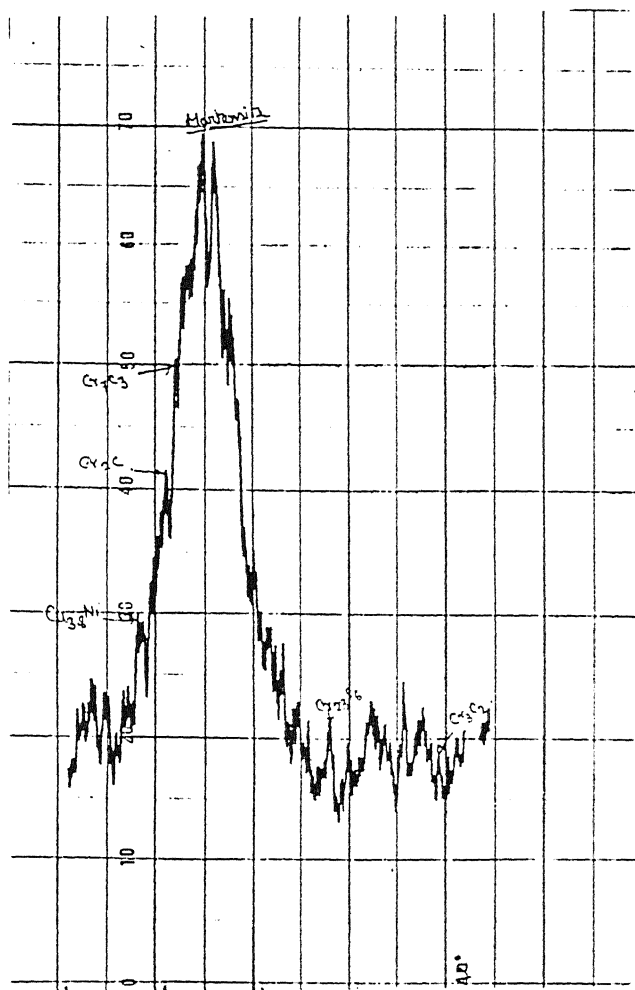


Figure 4.2: X-Ray chart for the sample A3

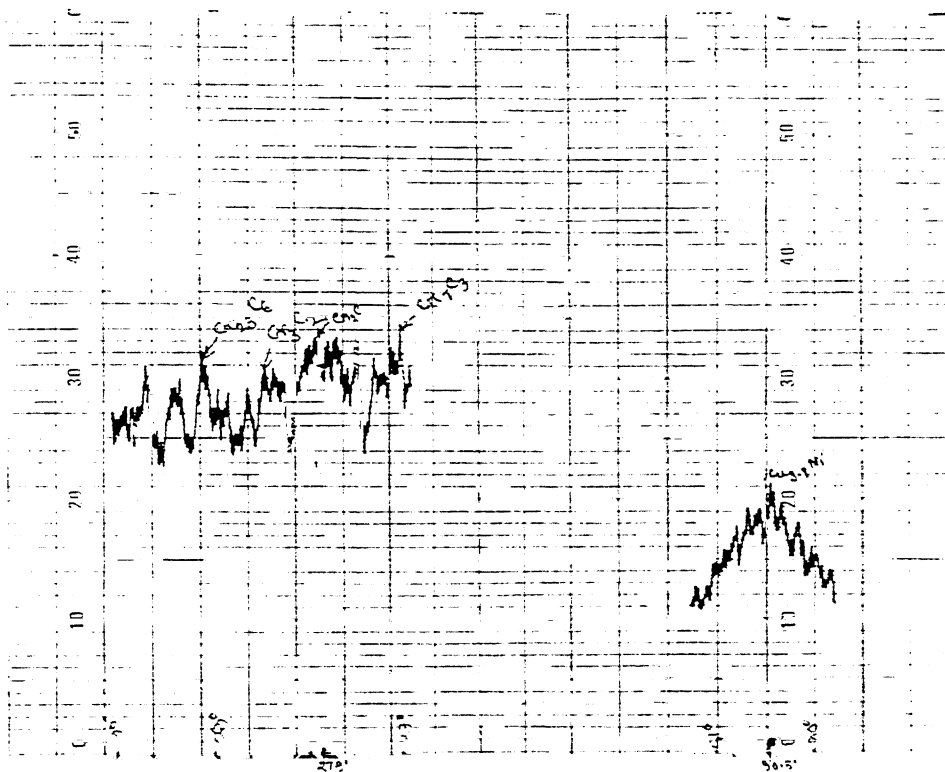


Figure 4.3: X-Ray chart for the sample C1

| Different phases present | Height of 100% intensity of different phases(cm) | I_{max}/I_{phase} |
|--------------------------|--|---------------------|
| $Cu_{3.8}Ni$ | 1.0 | 0.165 |
| Cr_2C | 4.17 | 0.690 |
| Cr_7C_3 | 2.17 | 0.359 |
| Cr_3C_2 | 6.04 | 1.0 |
| $Cr_{23}C_6$ | 1.25 | 0.207 |

Table 4.3: X-Ray Analysis Table For Sample A3

| Different phases present | Height of 100% intensity of different phases(cm) | I_{max}/I_{phase} |
|--------------------------|--|---------------------|
| $Cu_{3.8}Ni$ | 9.5 | 1.0 |
| Cr_2C | 2.5 | 0.263 |
| Cr_7C_3 | 3.26 | 0.343 |
| Cr_3C_2 | 2.67 | 0.278 |
| $Cr_{23}C_6$ | 4.58 | 0.482 |

Table 4.4: X-Ray Analysis Table For Sample C1

Ratios of height of the 100% intensity of different precipitate phases with respect to maximum precipitated phases are given in table-4.4.

4.2.4 Analysis from X-Ray Data of the sample C3

Thermomechanical treatment of the sample: Soaking at 1080°C for 1h → 30% rolling at 1080°C → Air cooling → Ageing for 18h at 580°C

X-Ray chart for this sample is shown in Fig.4.4.

From X-Ray chart it is clear that precipitates are of the following types- 1. $Cu_{3.8}Ni$ 2. Cr_2C 3. Cr_3C_2 4. Cr_7C_3

Height of the 100% intensity of the different precipitating phases with respect to height of 100% intensity of the maximum precipitating

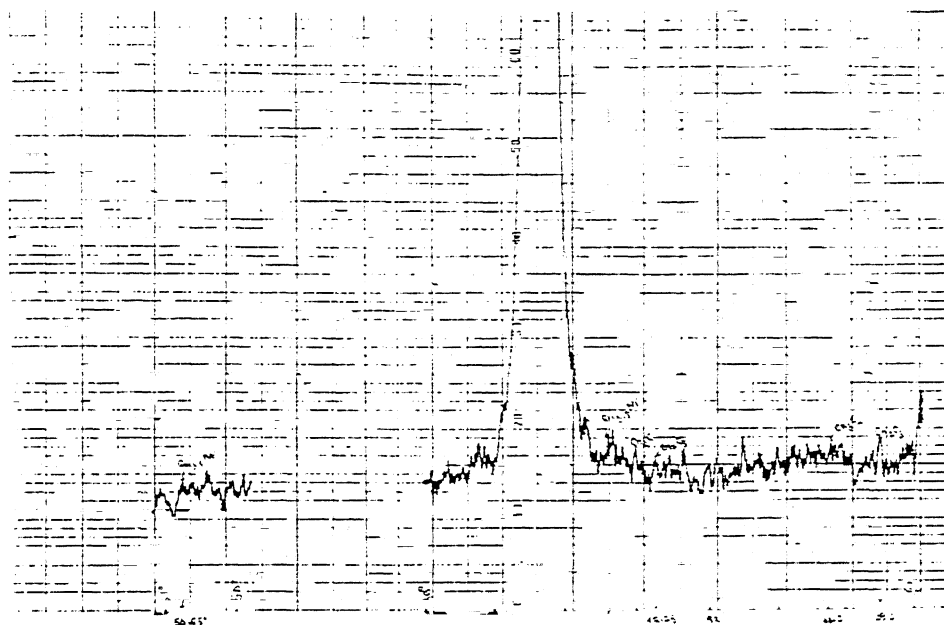


Figure 4.4: X-Ray chart for the sample C3

| Different phases present | Height of 100% intensity of different phases | I_{max}/I_{phase} |
|--------------------------|--|---------------------|
| $Cu_{3.8}Ni$ | 0.85 | 0.391 |
| Cr_2C | 2.16 | 0.995 |
| Cr_7C_3 | 2.17 | 1.0 |
| Cr_3C_2 | 1.67 | 0.769 |

Table 4.5: X-Ray Analysis Table For Sample C3

phase are given in table-4.5.

4.2.5 Analysis from X-Ray Data of the sample P1

Thermomechanical treatment of the sample: Soaking at $1080^{\circ}C$ for 1h
 - \rightarrow 40% rolled at temperature $1080^{\circ}C$ - \rightarrow Natural ageing

X-Ray chart for this sample is shown in Fig.4.5.

From X-Ray chart it is clear that natural ageing is very slow in this type of steel even after giving a high percentage deformation which is also very clear from the SEM microstructure of this sample. (where)?

4.2.6 Analysis from X-Ray Data of the sample D1

Thermomechanical treatment of this sample: Soaking at $1080^{\circ}C$ for 1h
 - \rightarrow Air cooling - \rightarrow 50% deformation at temperature $300^{\circ}C$ - \rightarrow Ageing at temperature $300^{\circ}C$ for 18h

X-Ray chart for this sample is shown in Fig.4.6-4.10. It is showing that ageing at low temperature gives complex carbide of the form $(Cr,Fe)_7C_3$. But no other precipitate can form at that temperature.

\rightarrow From all the X-Ray charts and the tables of 100% intensity of the different precipitating phases with respect to 100 that Cr_2C is the phase which is precipitated first and it gradually transforms into Cr_3C_2 , Cr_7C_3 and $Cr_{23}C_6$. But $Cr_{23}C_6$ can only be precipitated out at highly deformed samples. More and more $Cu_{3.8}Ni$ is precipitated out as the percentage deformation increases at high temperature such as $1080^{\circ}C$. But the effect of deformation on precipitation of $Cu_{3.8}Ni$ is

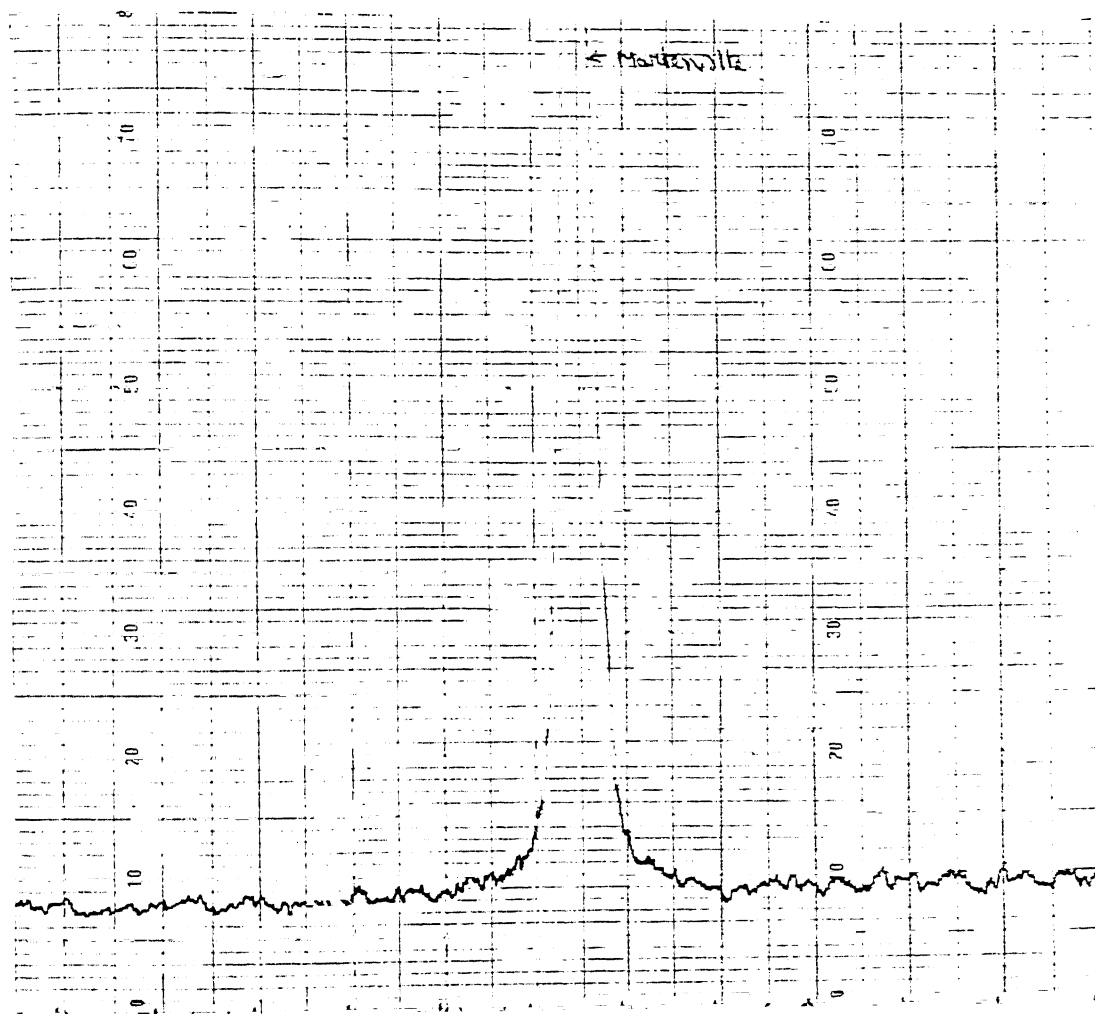


Figure 4.5: X-Ray chart for the sample P1

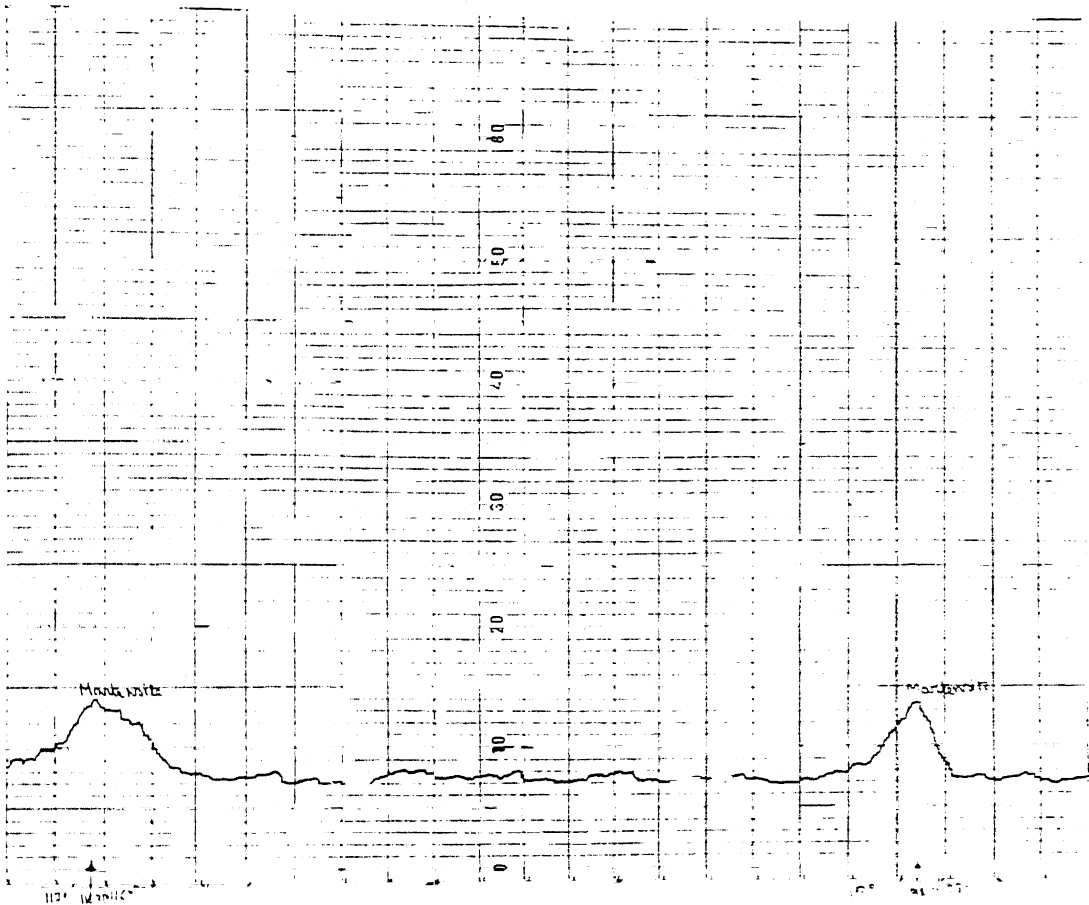


Figure 4.6: X-Ray chart for the sample D1

| Phases present | I_{max}/I_{phase} For 30% Rolling | I_{max}/I_{phase} For 70% Rolling |
|----------------|--|--|
| Cr_2C | 0.995 | 0.263 |
| Cr_3C_2 | 0.769 | 0.278 |
| Cr_7C_3 | 0.343 | 1.0 |
| $Cr_{23}C_6$ | 0.482 | 0 |
| $Cu_{3.8}Ni$ | 0.391 | 1.0 |

Table 4.6: Comparison Of Various X-Ray Analysis Results

more intense at that high temperature than on precipitation of $Cr_{23}C_6$. These points are clear from the table-4.6.

4.3 Analysis of the SEM Microstructures

Microstructure of the as received sample is shown in fig.4.11. The microstructure shows the precipitate particles in martensitic matrix.

Microstructures for the samples which are rolled at high temperature prior to ageing at $580^\circ C$ are shown in fig 4.14-4.18. From the microstructure of the sample which is 70% rolled it is clear that some precipitate particles are very small. Cu and Ni gives coherent precipitates of the type $Cu_{3.8}Ni$ which are very small in size. From microstructures it is also clear that as the percentage deformation increases more and more small particles are formed which is also supported by X-Ray analysis. It is also clear from the microstructures that as the percentage deformation increases more and more precipitates get distributed throughout the volume. More deformation produces more strain hardened sites which act as nucleation sites for precipitation. Microcracks are also present in the structures.

It is clear from the microstructures of the sample aged at temperatures $580^\circ C$ and $480^\circ C$ which are shown in fig 4.12-4.26 that at $480^\circ C$ volume fraction of the precipitates is very low because precipitation of chromium carbides are favoured by high temperature.

Microstructure of the fully aged sample without any deformation is shown in fig 4.19.

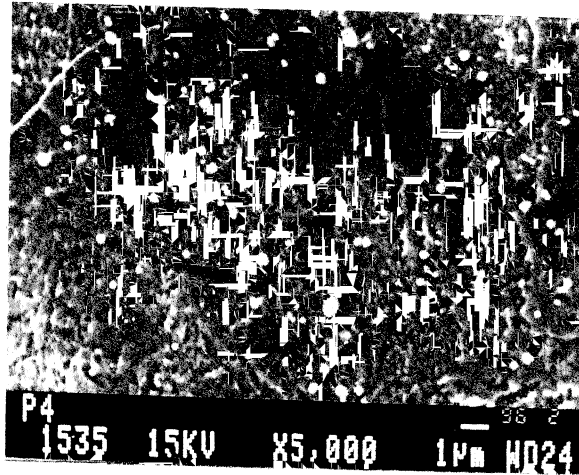


Figure 4.11: Microstructure of the as received sample

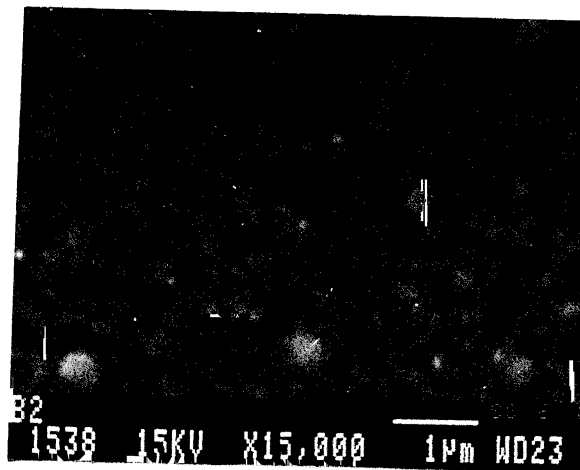


Figure 4.12: Microstructure of the sample which is 50% rolled at 1080°C and aged at 480°C

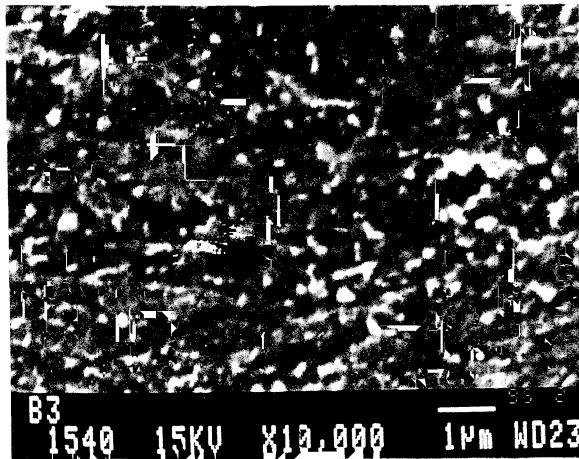


Figure 4.13: Microstructure of the sample which is 70% rolled at 1080°C and aged at 480°C

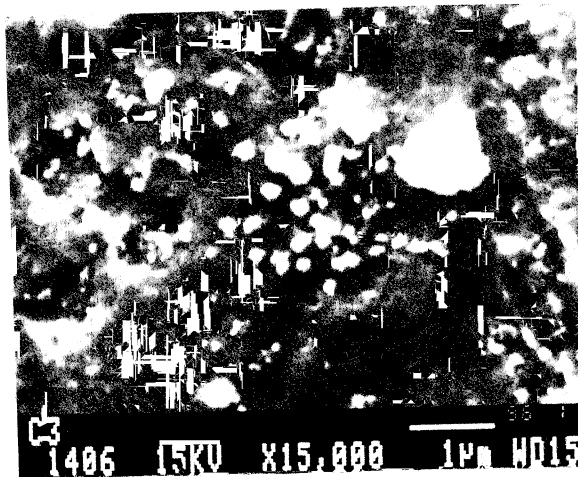


Figure 4.14: Microstructure of the sample which is 70% rolled at 1080°C and aged at 580°C

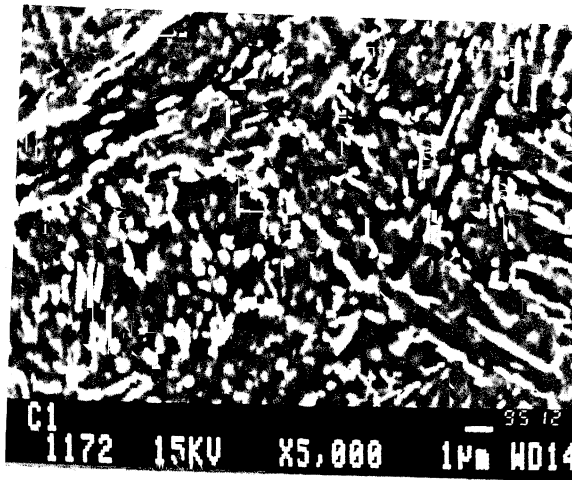


Figure 4.15: Microstructure of the sample which is 30% rolled at 1080°C and aged at 580°C

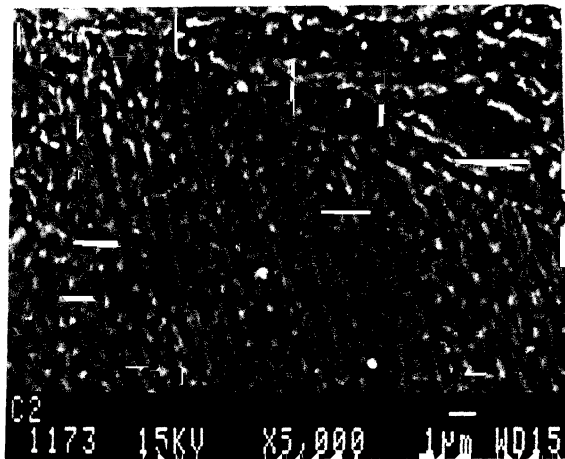


Figure 4.16: Microstructure of the sample which is 50% rolled at 1080°C and aged at 580°C

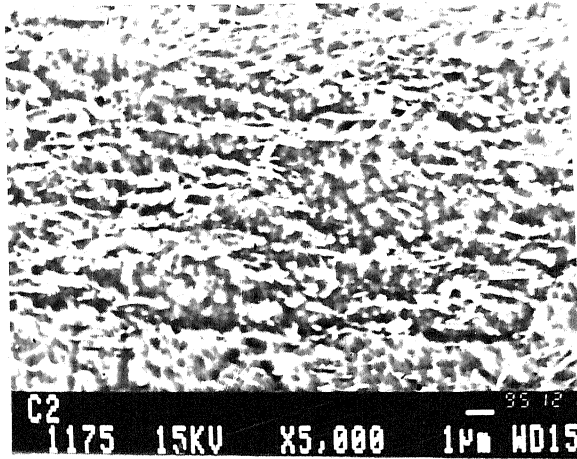


Figure 4.17: Microstructure of the sample which is 50% rolled at 1080°C and aged at 580°C

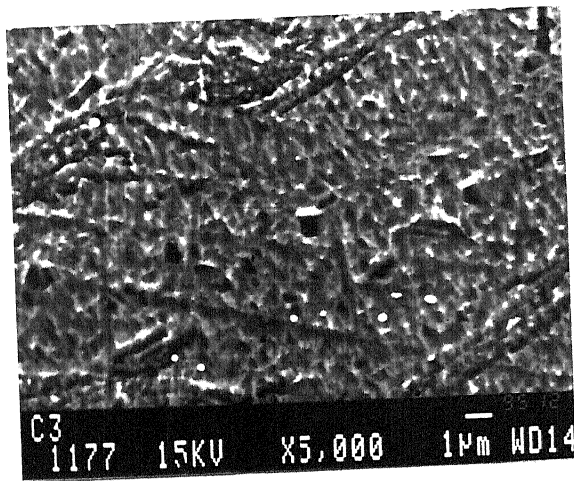


Figure 4.18: Microstructure of the sample which is 70% rolled at 1080°C and aged at 580°C

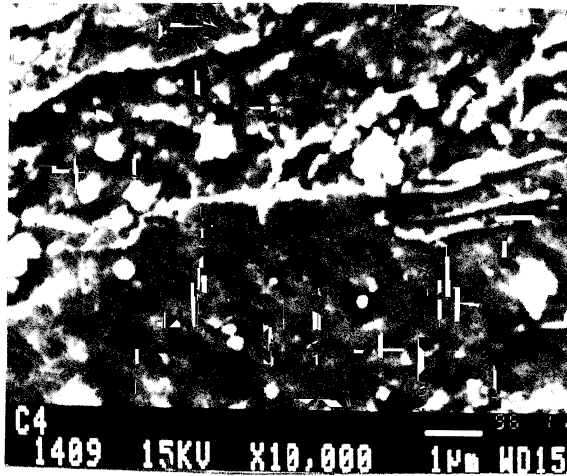


Figure 4.19: Microstructure of the sample which is aged at 580°C

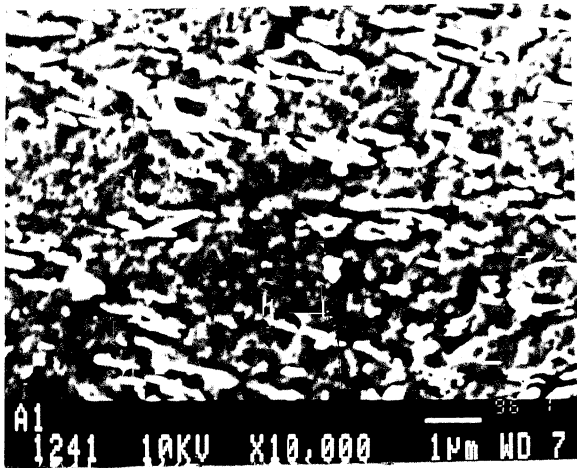


Figure 4.20: Microstructure of the sample which is aged and rolled to 30% at 580°C

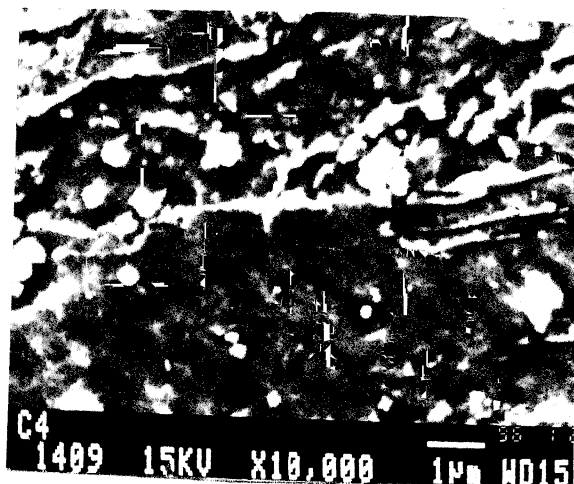


Figure 4.19: Microstructure of the sample which is aged at 580°C

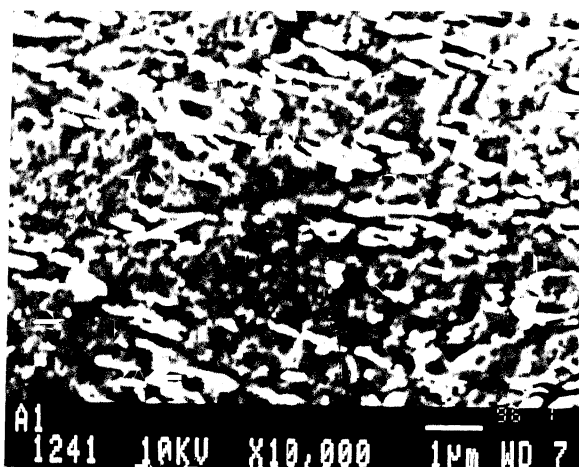


Figure 4.20: Microstructure of the sample which is aged and rolled to 30% at 580°C

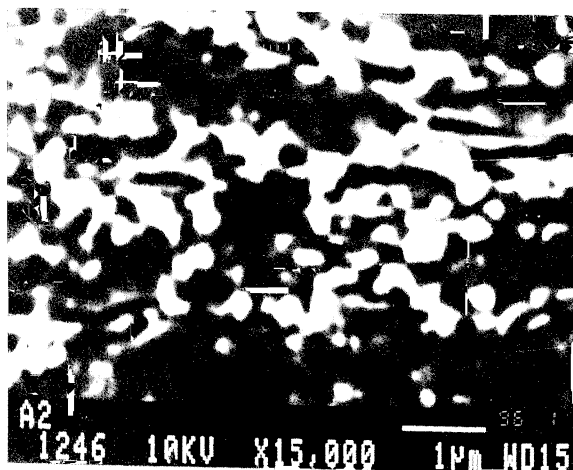


Figure 4.21: Microstructure of the sample which is aged and rolled to 50% at 580°C

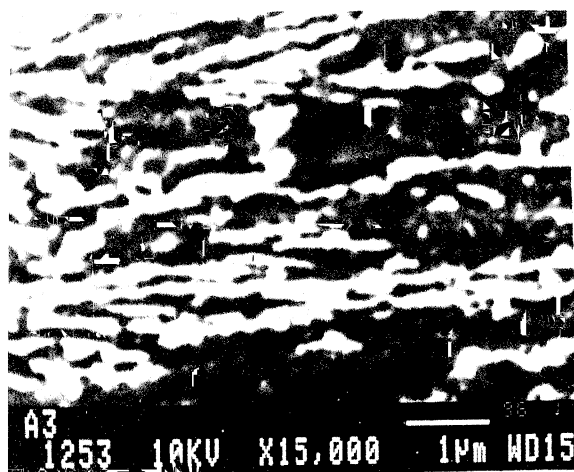


Figure 4.22: Microstructure of the sample which is aged and rolled to 70% at 580°C

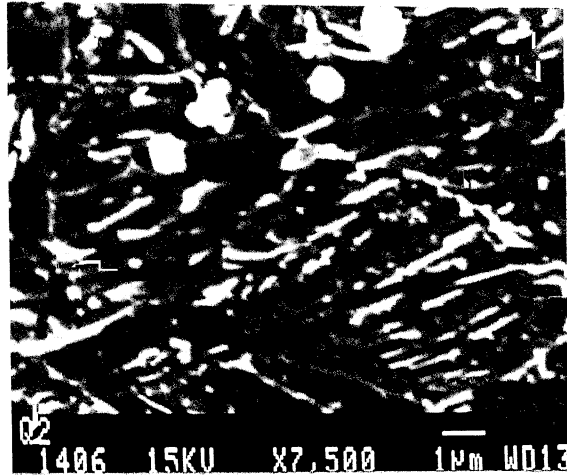


Figure 4.23: Microstructure of the sample which is aged and rolled to 30% at 480°C

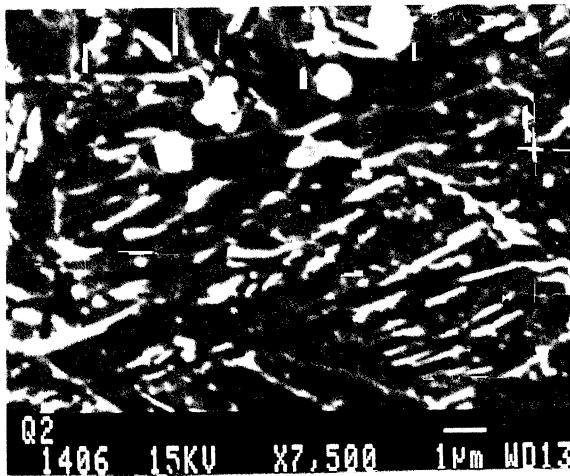


Figure 4.24: Microstructure of the sample which is aged and rolled to 50% at 480°C

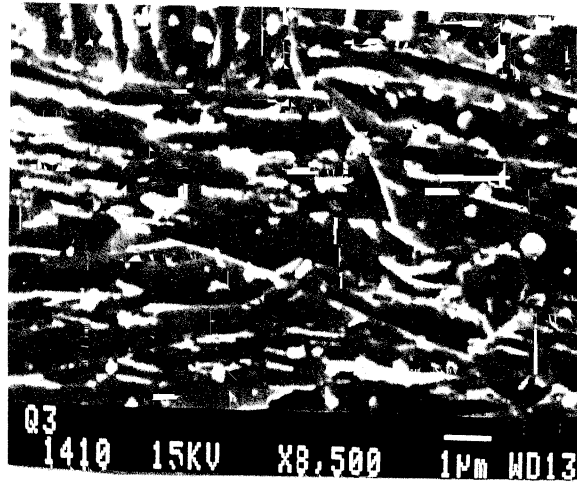


Figure 4.25: Microstructure of the sample which is aged and rolled to 70% at 480°C

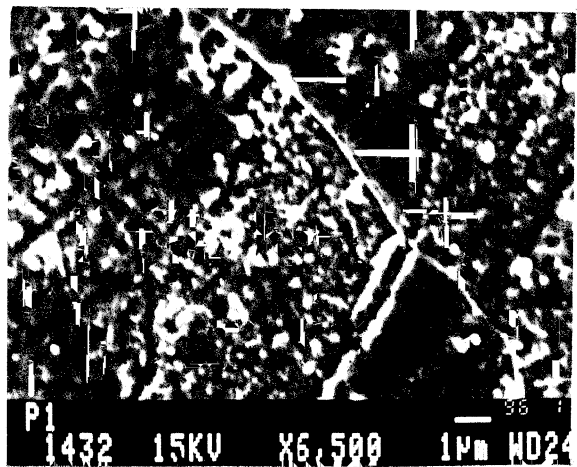


Figure 4.26: Microstructure of the sample which is 40% rolled at 1080°C and naturally aged

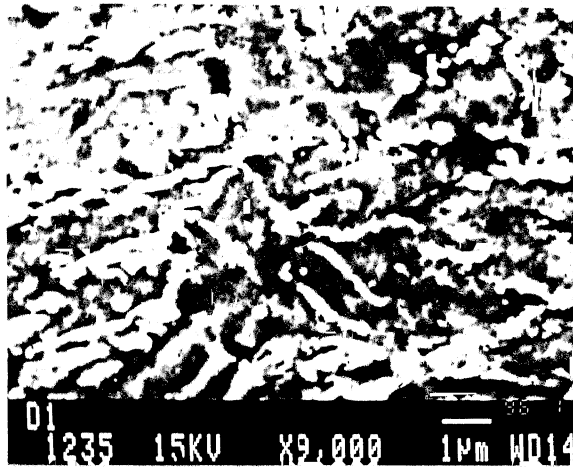


Figure 4.27: Microstructure of the sample which is rolled to 50% and aged at 300°C

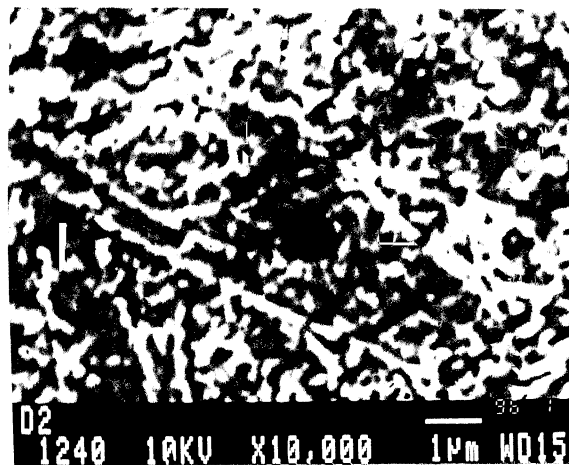


Figure 4.28: Microstructure of the sample which is rolled to 30% and aged at 300°C

Microstructures for the samples rolled after aged at 580°C are shown in fig 4.20-4.22. A long crack path is shown in fig. 4.22 for the sample to which maximum deformation is given. From the microstructures of the sample which are rolled after aged at 480°C it is clear that longer cracks are formed as the percentage increases.

The microstructures of the samples which are naturally aged after rolled at high temperature is shown in fig. 4.26. It shows that natural ageing occurs at very small extent in this steel even after giving a high percentage deformation which is also clear from X-Ray chart.

The microstructures of the sample which are aged after rolled at 300°C are shown in fig 4.28-4.29 which shows complex precipitates of the type $(\text{Cr},\text{Fe})_7\text{C}_3$.

*↑ where are cracks?
where is 4.29*

4.4 Results Obtained from Hardness Measurement

From the micro-hardness data it is clear that as the temperature of ageing increases, hardness value increases. With increasing percentage deformation hardness values also increase. With highest percentage deformation i.e. 70% and high temperature (580°C) ageing it gives maximum hardness (Fig. 4.30 and 4.31). Maximum

hardness is obtained in that condition because of the presence of $\text{Cu}_{3.8}\text{Ni}$ intermetallic phase. Even 30% rolling at 1080°C gives high hardness value compared to values obtained from samples treated in different conditions due to presence of this intermetallic phase. The samples rolled and aged at 300°C give high hardness due to presence of the complex carbides of the type $(\text{Cr},\text{Fe})_7\text{C}_3$. All these results are clear from the Fig. 4.30-4.31. The curves dp.1, pd.1 represent 30% rolled samples. The curves dp.2, pd.2 represent 50% rolled samples. The curves dp.3, pd.3 represent 70% rolled samples. The hardness values obtained are given in tables-4.7 and 4.8.

Crystal structures of the precipitates are of the following types-

1. $(\text{Cr},\text{Fe})_7\text{C}_3 \rightarrow$ Hexagonal. $a=13.98, c=4.523$
2. $\text{Cu}_{3.8}\text{Ni} \rightarrow$ Cubic. $a=3.595$

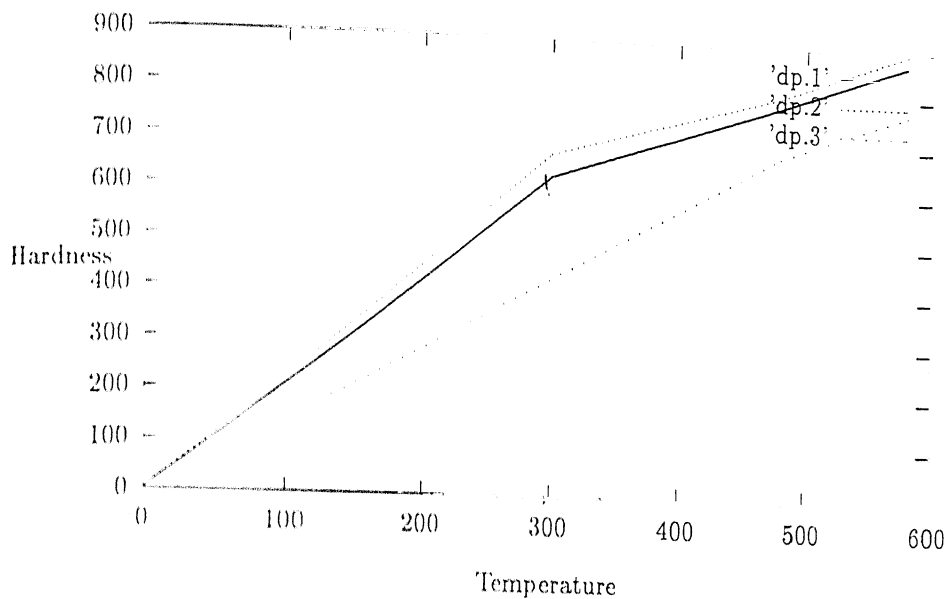


Figure 4.29: Hardness Vs. Ageing Temperature Plot For The Samples Which Are First Rolled And Then Aged

| Ageing Temp. In °C | HV For 30% Rolled Samples | HV for 50% Rolled Samples | Hv For 70% Rolled Samples |
|-----------------------|---------------------------------|---------------------------------|---------------------------------|
| 300 | 627 | 673 | — |
| 480 | 780 | 800 | 880 |
| 580 | 870 | 894 | 920 |

Table 4.7: Hardness Values For First Rolled And Then Aged Samples

| Ageing Temp. IN °C | HV for 30% Rolled Samples | HV for 50% Rolled Samples | HV for 70% Rolled Samples |
|-----------------------|---------------------------------|---------------------------------|---------------------------------|
| 480 | 681 | 707 | 743 |
| 580 | 772 | 792 | 813 |

Table 4.8: Hardness Values For First Aged And Then Rolled Samples

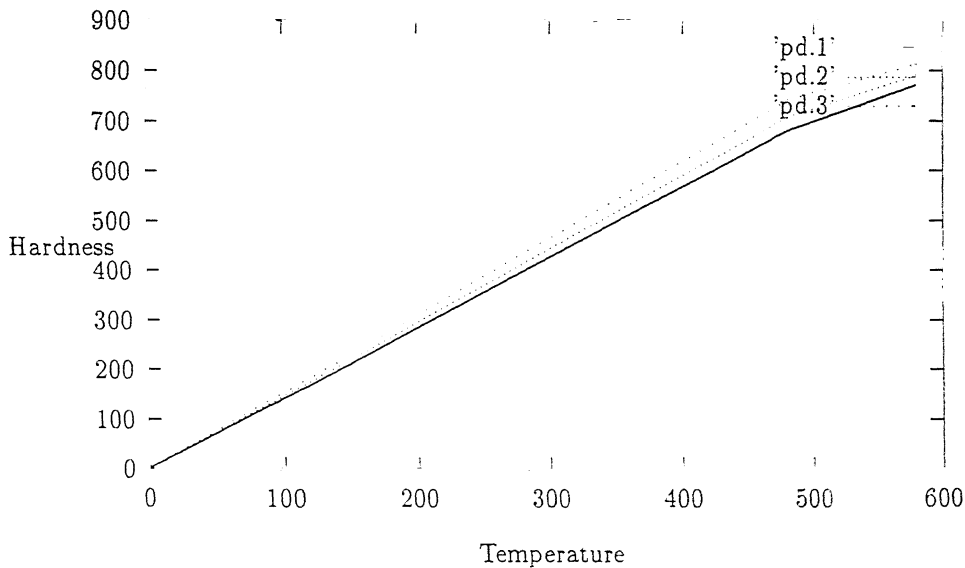


Figure 4.30: Hardness Vs. Ageing Temperature Plot For The Samples Which Are First Aged And Then Rolled

3. Cr_2C → orthorhombic. $a=7.0149, b=12.153, c=4.5320$
4. Cr_3C_2 → Hexagonal. $a=2.79, c=4.46$
5. Cr_7C_3 → Orthorhombic. $a=5.5273, b=11.4883, c=2.8286$
6. Cr_{23}C_6 → Cubic $a=10.6599$

→ Since lattice parameter of $\text{Cu}_{3.8}\text{Ni}$ is nearer to length of c axis of martensite ($c=3.018$) it gives small coherent precipitates which are identified in the SEM microstructures. Cr_2C precipitates are also coherent because their "a" value ($a=2.79$) matches with "a" value of martensite ($a=2.847$).

Highest hardness value obtained in case of samples rolled at 1080°C can be explained with the help of the theory suggested by Mott and Nabarro[4]. To give close matching across the interface between the martensitic matrix and $\text{Cu}_{3.8}\text{Ni}$ it generates regions of misfit stresses. Due to presence of these high strained regions it gives high hardness values.

As percentage deformation increases more and more dislocations are produced in the samples. Glide dislocations pass through the precipitate by cutting it or by-passing it. Coherent precipitates with low surface energy can easily be sheared. Non-coherent precipitates have high surface energy and cannot be easily sheared. Since most of the

→ precipitates are of different crystal structures with respect to martensite, ~~so~~ slip planes are not continuous from martensite to precipitates. For this reason dislocation by-pass the precipitates by creating jogs. If it is not possible for the dislocation to cut through or by pass the precipitate then due to high stress particles get decohesed from the matrix by creating voids. Both voids and cracks are present in the microstructures.

He used a
word in Eng
lang

Chapter 5

CONCLUSIONS

Results of the present study on 174PH stainless steel help in drawing the following conclusions-

1. Precipitates are of various chromium or iron chromium carbides and the intermetallic compound $\text{Cu}_{3.8}\text{Ni}$. Though no intermetallic compound is observed in binary Cu-Ni phase diagram, it appears that formation of these intermetallic compound is favoured by presence of other elements as in case of 17-4PH.
2. Precipitation behaviour in 17-4PH stainless steel is strongly influenced by processing parameters.
3. Rolling at 1080°C gives intermetallic phase $\text{Cu}_{3.8}\text{Ni}$. However at lower rolling temperature precipitation of $\text{Cu}_{3.8}\text{Ni}$ is not observed. Volume fraction of $\text{Cu}_{3.8}\text{Ni}$ increases as the percentage deformation increases.
4. Cr_2C is the phase which is precipitated first. With progress of ageing it gradually transforms to Cr_7C_3 and Cr_{23}C_6 irrespective of their rolling temperature.
5. However Cr_{23}C_6 can only be precipitated out at highly deformed samples. Effect of deformation on precipitation of $\text{Cu}_{3.8}\text{Ni}$ is more than on precipitation of Cr_{23}C_6 .
6. Ageing at lower temperature such as 300°C gives rise to formation of complex precipitates of the type $(\text{Cr,Fe})_7\text{C}_3$. No other precipitate can form at this temperature.

7. Natural ageing is very slow in this type of steel even after giving a high percentage deformation.
8. Hardness of the aged 17-4 PH stainless steel increases as temperature of ageing and percentage deformation increases. Highest hardness is obtained from the sample rolled and aged at high temperature due to the presence of the $\text{Cu}_{3.8}\text{Ni}$ intermetallic phase.

REFERENCES

1. F.B.Pickering et al.:International Metals Reviews,December 1976,1
2. I.Novikov:"Theory of Heat Treatment of Metals",307-312
3. I.Novikov:"Theory of Heat Treatment of Metals",314-319
4. Mott,N.F. and Nabarro.F.R.N., Proc. Phy. Soc.,52(1940),86:
Report on conf. Strength of Solids.Physical Society.(1948)1
5. Kelly, A., "Electron Microscopy and Strength of Crystals" (Thomas.G.
and Washburn.J.,Eds.)Interscience.New York.(1963) 947
6. Nicholson.R.B.,Thomas.G. and Nutting,J.,J. Inst. Metals, 87(1958-
59)429
7. Price,R.J. and Kelly,A.,Acta Met.,11(1963)915;12(1964)159
8. Nicholson.R.B. and Nutting,J.,Acta Met.,9(1961)332
9. Chun,J.C. and Byrne,J.G.,J. Mat. Science,4(1969)861
10. Fleischer.R.L.,ibid,p.973
11. Fleischer.R.L.,Acta Met.,8(1960)598
12. Koda,S.,Matsuura.K. and Takahasi,N.,J. Inst.Metals. 91(1962-
63)225
13. Fleischer.R.L.,Acta Met.,9(1961)996
14. Gerold,V. and Hoberkorn.H.,Phy. Stat. Soli.,16(1966)675
15. Raynor,D. and Silcock,J.M.,Metal Sci. J.,4(1970)121
16. Hirsch,P.B. and Kelly,A.,Phil. Mag.,12(1965)881
17. Van Aswegen,J.S.T.,Honeycombe,R.W.K. and Warrington, D.H.,Acta
Met.,12(1964)1
18. Van Aswegen,J.S.T. and Honeycombe,R.W.K.,Acta Met.,10 (1962)262
19. Silcock,J.M.,J. Iron and Steel Inst.,201(1963)409

20. Silcock, J.M. and Tunstall, W.J., *Phil. Mag.*, 10(1964)361
21. Naybour, R.D., *J. Iron and Steel Inst.*, 204(1966)1200
22. Harding, H.J. and Honeycombe, R.W.K., *J. Iron and Steel Inst.*, 204(1966)259
23. Hirsch, P.B., *J. Inst. Metals*, 86(1957-58)13
24. Orowan, E., *Symp. Internal Stresses in Metals and Alloys. Inst. of Metals, London*, (1948)451
25. Ansell, G.S. and Lanel, F.V., *Acta Met.*, 8(1960)612
26. Tanaka, K. and Mori, T., *Acta Met.*, 18(1970)931
27. Ashby, M.F., *Phil. Mag.*, 14(1966)1157
28. Tanaka, K., Mori, T. and Nakamura, T., *Phil. Mag.*, 21(1970)267
29. Hosford, W.F., Fleischer, R.L. and Backofen, W.A., *Acta Met.*, 8(1960)18
30. Byrne, J.G., Fine, M.E. and Kelly, A., *Phil. Mag.*, 6(1961)1119
31. Fisher, J.C., Hart, E.W. and Pry, R.H., *Acta Met.*, 1(1953)336
32. Mott, N.F., *Phil. Mag.*, 1(1956)568
33. Avner, H.: "Introduction To Physical Metallurgy", 374-376
34. Pickering, F.B., "Precipitation processes during the tempering of martensitic alloy steels", *Precipitation Processes in Steels* (The Iron and Steel Institute, 1959), 23-26
35. Allen, P.M., *Iron Age*, V.180 n2, July 11, (1957)99-101
36. Monypenny, J.H.G., "Stainless Iron And Steel" (Vol.2), Chapman and Hall Ltd. (1954), 161
37. Schneider, H.: *Foundry Trade J.*, 1960, 108